NASA Contractor Report 165626

STUDIES ON PROPER SIMULATION DURING STATIC TESTING OF FORWARD SPEED EFFECTS ON FAN NOISE

A.A. Peracchio, U.W. Ganz,

M. Gedge and K. Robbins

UNITED TECHNOLOGIES CORPORATION

Pratt & Whitney Aircraft Group
Commercial Products Division
East Hartford, Connecticut 06108

and

Boeing Commercial Airplane Company
Seattle, Washington 98124

Contract No. NAS1-15085
September 1980

National Aeronautics and
Space Administration
Langley Research Center
Hampton, Virginia 23665

TABLE OF CONTENTS

PRECEDING PAGE BLANK NOT FILMED

iii

ACKNOWLEDGEMENTS

iv

1.0 SUMMARY

Significant differences exist in the fan tone noise generated by engines in flight and engines operating on the test stand. It has been observed that these differences are reduced by the use of an Inflow Control Structure (ICS) in the static test configuration. It is the purpose of this contract (NAS1-15085) to produce a design system for ICS's, to provide a methodology for projecting the resulting data to flight and to assess the design system and projection methodology by comparing static data, obtained from a JT9D tested with an ICS and then projected to flight, with flight data from a Boeing 747 equipped with JT9D engines.

The contract consisted of three phases. Results from Phase I and Phase II are described in References 1, 2 and 3 and are summarized briefly in this final report. The results of Phase III are described herein.

The atmospheric model from Phase I and the models accounting for the effects of contraction and screening on inflow distortion are combined in Phase II to provide an ICS design system. This design system was then assessed by predicting and comparing the inflow characteristics at the fan face of a JT9D engine to the inflow characteristics deduced from Blade Mounted Transducer Data.

Based on Contractor experience, test procedures for static testing with an ICS and corrections required to project this data to flight were defined. The ICS design system and the test and projection procedures were then combined into a procedures report which is included in Appendix I.

Assessment of the procedures report was accomplished by projecting to flight, static data obtained from a JT9D engine tested with an ICS, and comparing these results with flyover data. The assessment showed that, on the average, for the four speeds (which span approach to takeoff operating conditions) and for the range of measurement angles considered (20^0 to 140^0 from the inlet centerline), use of an ICS improved agreement between projected static and measured flyover data by 3.1 dB for the BPF one third octave band (1/3 OB) tone level. Without an ICS, on the average, static BPF data projected to flight were about 3.9 dB higher than flight data. With an ICS, this difference was reduced to 0.8 dB.

2.0 INTRODUCTION

Reduction of aircraft engine noise levels is a continuing process which has resulted in significant noise reduction since the advent of the original commercial jet aircraft in the early 1950's. Engine noise reduction features are usually verified by means of static or flight testing. Since the cost of flight testing is much greater than that of static testing, use of the latter technique results in significantly lower costs being accrued to the development of engine noise reduction features. As such, the use of static testing techniques should be fully exploited. The purpose of this contract is to further develop static test technology for turbofan noise studies.

It has been noted by various observers that the noise produced by the fan of some turbofan engines operating statically on the test stand is greater than that produced when the engine is operating under flight conditions. This may be a result of both fan blade passing tone and broadband levels being contaminated by extraneous noise sources present during static testing. As a consequence, predictions of flight noise levels using static data are high. Depending on the engine type, it is also possible that flight noise sources cannot be identified from noise data acquired in static tests, and therefore, noise reduction techniques cannot be evaluated on the test stand in the presence of contaminating extraneous noise. To identify the source of extraneous noise it is necessary to note that, statically, the fan interacts with a more distorted inflow field than it does when in flight. There are several features of the inflow field that are quite different when the engine is operating statically, each of which could produce extraneous noise.

Firstly, the intensity of the atmospheric turbulence in the vicinity of the ground is higher than at higher altitudes. In addition, this turbulence field is convected through a very high flow contraction when the engine is operating statically, whereas, in flight, the turbulence field convects through a very small contraction on its way to the fan. This high flow contraction in the static case results in a distortion of the turbulence field in which the "eddies" are "stretched", then "chopped" by successive fan blades, producing "bursts" of discrete tone noise that are virtually absent in the flight operation of the engine.

2

Secondly, in the static case, the stand structure and the ground plane are sources of flow disturbances. Engine ingested air passes over the stand structure and the ground resulting in vortices and wakes in the inflow field. Exterior engine case protuberances can also generate ingestible distortions. Usually these sources of distortion do not exist in flight since the air ingested into an engine has not passed over any exterior surfaces.

Thirdly, the nacelle boundary layer, because of differences in the mean flow between static and flight, is different during static operations of the engine.

Finally, since it is possible for the flow to be drawn from all angles by an engine on the test stand, turbulent flows from the jet plume may be reingested. This distortion source is not present in flight.

The disturbances described above (i.e., atmospheric turbulence, ground plane and stand induced distortions, dissimilar nacelle boundary layer and jet plume reingestion) are considered to be the most important extraneous noise sources in static engine operation. In order to obtain useful static acoustic data, it is therefore necessary to develop techniques which modify the inflow field so that the fan is operating as it would in flight. In the past, various techniques for accomplishing this simulation have been used, including mounting engines in wind tunnels and using devices upstream of the fan to condition the inflow. Inflow Control Structures (ICS) for conditioning the flow have been mounted upstream of the engine by several investigators. This technique has resulted in reduced radiated noise levels, indicating the reduction of inflow distortion. In view of the encouraging results achieved by the use of ICS's, the present contract was awarded for the purpose of developing an interim Procedures Report, to include an inflow control screen design procedure and a flight noise prediction procedure using data gathered from the static testing of engines equipped with such a structure. Additionally, the procedures have been assessed using static data from a Pratt & Whitney Aircraft (PWA) JT9D engine equipped with an ICS and flyover data from a Boeing 747 airplane equipped with JT9D engines. These data were obtained during a joint Boeing/ Pratt & Whitney program and were provided as part of the contract.

The major components of the contract are:

Phase I Definition of Atmospheric Turbulence Characteristics and Engine Sensitivity Study.

Phase II Development of Inflow Control Structure (ICS) Preliminary Design System.

Phase III Interim Procedures Report Development and Coordination.

The results of Phase I and Phase II have been described in References 1, 2 and 3, but parts that are pertinent to the Phase III effort are summarized in this report. The results of Phase III are described in this report, and the Interim Procedures Report is contained in Appendix I.

4

3.0 SYMBOLS AND ABBREVIATIONS

ANOPP	Aircraft noise prediction program
BPF	Blade passage frequency
BPF_m	Blade passage frequency sound pressure level measured during a single flyover.
BPF_{ma}	Average of blade passage frequency sound pressure level for several flyovers.
BPF_p	Predicted blade passage frequency sound pressure level based on averaged static data.
BPF_{pI}	Predicted blade passage frequency sound pressure level based on averaged static data obtained with an inflow control structure.
BPF_{pNI}	Predicted blade passage frequency sound pressure level based on averaged static data obtained without an inflow control structure.
$(BPF_{ma}-BPF_{pI})_a$	Average over all measurement angles of the quantity $(BPF_{ma} - BPF_{pI})$
$(BPF_{ma}-BPF_{pNI})_a$	Average over all measurement angles of the quantity $(BPF_{ma} - BPF_{pNI})$.
dB	Decibel $\left[20 \log (\text{sound pressure} / 2 \times 10^{-5} \text{ N/M}^2) \right]$
FAA	Federal Aviation Administration
HBPR	High bypass ratio
ICS	Inflow control structure
NASA	National Aeronautics and Space Administration
OB	Octave Band
PNL	Perceived noise level
PWA	Pratt & Whitney Aircraft

4.0 INTERIM PROCEDURES REPORT DEVELOPMENT (PHASE III)

4.1 Review of Phase I and Phase II Results (Phase III, Task A)

Under Phase I, atmospheric turbulence characteristics were defined and a study was conducted to determine the sensitivity of engines of various sizes to inflow distortion scale. The PWA JT9D and JT15D engines were selected for the sensitivity study. Details of the work performed in Phase I are given in Reference 1. In Phase II, analytical models for contraction and screening effects on turbulence and steady distortion were developed. In addition, a test program was conducted to experimentally define the effects of contraction and screening on turbulence and steady distortion. The effects of the ICS on acoustic transmission were studied analytically and experimentally. The analytical models and experimental results were combined to provide semiempirical models for the development of an ICS design system, and to show that transmission effects connected with well designed ICS's are small and can be neglected. These studies are described in detail in References 2 and 3.

A brief review of the results from Phases I and II that are pertinent to the ICS design system are given below.

The atmospheric turbulence intensities and length scales that exist during static testing and in flight can be obtained from the results of Reference 1 as a function of altitude above the ground, mean wind velocity, surface roughness and atmospheric stability.

Analytical studies of rotor-turbulence interactions show that the mechanism is dominated by distortion elements within a small range of transverse scales. For typical turbulence energy distributions encountered in the atmosphere this range covers about one decade and is centered around a transverse scale in the order of 30% of the rotor blade spacing at the blade tip. For a given turbulence variance, maximum sound power levels are achieved at transverse integral scales in the order of 25% of the rotor blade spacing at the blade tip. For a JT9D fan this is about 4.1 cm and for the JT15D fan it is about 1.3 cm.

6

Based on the atmospheric turbulence model and the analytical contraction
models from Reference 1, the prediction of rotor-turbulence interaction noise
statically and in flight for JT9D and JT15D sized engines shows that tone
levels at approach power are on the order of 30 dB higher under static condi-
tions than they are in flight. This points out the importance of suppressing
the rotor-atmospheric turbulence interaction during static testing. Since the
rotor-turbulence interaction tone noise level is so low in flight, designing
ICS's to achieve flight levels of turbulence during static testing would
provide a conservative ICS design.

In considering steady distortions, it was shown in Phase II (Reference 3) that
the transverse velocity component of steady or quasi-steady distortions is not
suppressed by flow contractions. Since distortions with significant components
of transverse velocity can be generated by flow over the ground plane (e.g.
ground vortex), and, it is conjectured, by flow over the stand structure, it
is important to suppress these velocities with an ICS. Wakes with axial
velocity deficits are also generated by the test stand structure, and although
flow contraction tends to reduce these distortions, an ICS design should also
suppress steady axial velocity distortions. In order to provide a design goal,
it is necessary to specify the level to which the ICS should suppress the
steady distortions. Based on the studies described above, it was shown that in
flight levels of the turbulence involved in fan noise generation were so low
that the resulting fan tone noise was about 30 dB (based on an analysis band
width equal to 1 percent of BPF) below that generated under static conditions.
Furthermore, experimental data shows these static levels are about 5-10 dB
higher than typical fan tones generated with the turbulence suppressed. Thus,
the inflight rotor-turbulence interaction mechanism is on the order of 20 dB
below the fan generated noise levels. The inflight turbulence level therefore
provides a conservative target for which to aim the ICS design. Accordingly,
for both turbulence and steady inflow distortion suppression, the goal of the
ICS design will be to simulate inflight turbulence levels. This target is the
basis of the ICS design system developed in Phase II of the contract which is
discussed in Reference 3.

Assessment of the ICS design system using Blade Mounted Transducer (BMT) and hot film data from tests of a JT9D engine is described in Reference 3. Results of this assessment showed that, with an ICS, the blade inflow upwash velocity inferred from the BMT signals was 2-4 orders of magnitude greater than that predicted using the velocity prediction portion of the design system. This indicated that either the BMT signal level was set by disturbances other than the inflow velocity field (e.g., the local acoustic field) or that the prediction method was greatly in error. Further comparisons of the predicted velocity with hot film measurements showed much better agreement (the predicted being about one-half of the measured), supporting the prediction method, and suggesting that the BMT's in the presence of an ICS are responding to disturbances other than the blade inflow upwash velocity.

The effects of angle of attack on fan noise generation were studied in Phase I (Reference 1). Assessment of this problem was carried out using Pratt & Whitney Aircraft/Boeing joint noise program data obtained in a 747/JT9D flight test. The data used in the assessment included that from inlet, fan duct wall and fan blade mounted pressure transducers and fuselage mounted microphones. These data indicate that there is no obvious correlation between inlet angle of attack changes and changes in broadband noise as well as narrowband noise at BPF and its second and third harmonic. A circumferential variation of the buzzsaw sound pressure field in the inlet that increases with angle of attack has been observed. The acquired data did not allow the evaluation of inlet angle of attack effects on fan noise radiation.

4.2   Test Procedures and Corrections to Test Data (Phase III, Task B)

The test procedures recommended are part of the Procedures Report (Appendix I). These procedures are based on the contractor's experience, and are representative of those currently used in static engine noise testing. Corrections that account for acoustic fan tone propagation through the ICS were shown in Reference 3 to be small (i.e., less than 1 dB) if the fan speed is varied $\pm.5$ percent during the data recording phase of the test.

Inlet bellmouth design criteria are defined, and acoustic, meteorological and engine performance instrumentation are recommended. In addition, test condition recommmendations are made. These include recommended definitions of a

8

test point and techniques for controlling fan speed during the test period to
best simulate flyover data. Suggested limitations on temperature, humidity and
wind velocity are also included to insure that excessive atmospheric attenua-
tion does not occur, and to insure that acoustic data scatter is minimized by
wind shear gradients. A more detailed discussion of the test procedures and
effects such as three dimensional sound fields and fan nozzle area changes
between static and flight conditions is given in Appendix II. Also included in
the Procedures Report are suggestions for data acquisition and processing.
These encompass suggestions for tape recorders, system calibration and data
reduction.

The corrections used to project static data to flight are based on PWA and
Boeing experience in making flight predictions and analyzing flight data.
Included in these corrections are convective amplification and doppler shift
effects, corrections for ground reflections and extra ground attenuation and
corrections for spherical divergence and atmospheric absorption of sound.
Details on all of the above are given in Appendix I, The Procedures Report.

The accuracy of the flight predictions is studied in Section 4.4, where assess-
ment of the procedures manual is made by comparing predictions based on static
data from a JT9D engine tested with an ICS to flyover noise levels from a 747
equipped with JT9D engines.

4.3 Development of Procedures Report (Phase III, Task C)

The Procedures Report is based on the analytical and experimental studies con-
ducted as part of Phases I, II, IIIA and B and Pratt and Whitney and Boeing's
test and flight prediction experience. The Procedures Report consists of three
major parts. The first part describes the ICS design system, developed as part
of Phase II, Task G and discussed in Reference 3. The second part describes
static testing and data recording and analysis procedures (See Section 4.2).
The third describes procedures for projecting the measured, statically
obtained data to flight (See Section 4.2). The Procedures Report has been
prepared as a "stand alone" element of this final report and is contained in
Appendix I. As such, it can be used to design an ICS, define test procedures
for use with the ICS and project the resulting data to flight levels.

9

In developing the Procedures Report, techniques for projecting static data to flight were defined based on PWA and Boeing experience. The elements used to project static data to flight, with the exception of convective amplification, are contained in the ANOPP computer program developed by NASA Langley. In its current state, it cannot accept static data as input for subsequent projection to flight levels. Accordingly, it is suggested that NASA consider making the required changes. This would allow the projection to flight to be done by computer in a manner that is consistent with the ANOPP procedure.

4.4 Assessment of Procedures Report (Phase III, Task D)

The assessment of the Procedures Report was performed using static and flight data from the Boeing/PWA Joint Noise Program. The assessment was based on blade passage frequency (BPF) and twice blade passage frequency (2 BPF) 1/3 octave band tones since it is these components, in particular BPF, that are most affected by an ICS. These tones therefore provide the most critical assessment.

The assessment was performed by:

i)   extrapolating corrected static data for blade passage frequency (BPF) and its harmonic (2 BPF) to flight using the corrections defined in the procedures report.

ii) comparing the projected data for BPF and 2 BPF with the corresponding flight data.

The static data was obtained from a JT9D hardwalled engine tested with and without the PWA ICS. The engine with the ICS is shown in Figure 1. The flight data was obtained from flyovers of a Boeing 747 aircraft equipped with four hardwalled JT9D engines of the same model as that used in the static tests. Comparisons to flight were made for static data obtained with and without the ICS to assess the improvements in prediction* accuracy afforded by use of the ICS. The comparisons were made for BPF and 2 BPF data obtained from 1/3 octave band spectra, corrected to an FAA day (77°F, 70% RH).

---

* In this section, the words prediction and predicted are used to designate statically measured data projected to flight.

10

Figure 1   *Engine With Pratt & Whitney Aircraft Inflow Control Structure*

Flyover data were available for four flight conditions - approach 30° flap, approach 25° flap, takeoff and cutback. Two sets of static data were used to make the flyover noise predictions; one set was generated with the ICS installed and the other was generated without the ICS. Descriptions of the flyover test configurations are presented in Appendix III. Instead of presenting noise levels in terms of flyover time, they are presented in terms of the static measurement angles. Table I shows the relationship between flyover time and measurement angle for each of the four flight conditions.

TABLE I
FLYOVER TIME IN TERMS OF MEASUREMENT ANGLE

Time (Sec)

(Degrees)	Approach 30° Flap	Approach 25° Flap	Takeoff	Cutback
20	-4.24	-4.24	-11.6	-10.88
30	-2.29	-2.29	-5.2	-4.97
40	-1.43	-1.43	-3.17	-3.01
50	-.92	-.92	-2.10	-1.97
60	-.55	-.55	-1.40	-1.27
70	-.25	-.25	-.85	-.73
80	0.00	0.00	-.39	-.27
90	.25	.25	.03	.15
95	.37	.37	.23	.35
100	.49	.49	.44	.56
105	.62	.62	.65	.78
110	.75	.75	.87	1.00
115	.89	.89	1.10	1.23
120	1.05	1.05	1.35	1.48
130	1.40	1.40	1.91	2.04
135	1.62	1.62	2.24	2.38
140	1.87	1.87	2.62	2.76

Variability in the measured flyover data and predicted BPF levels, based on static data was also investigated. The flyover noise prediction at a particular angle is based on a curve which is spline fit, as a function of corrected speed, through measured static data at that angle, rather than on the static data points alone. The scatter of the measured data about this curve is a source of variability in the prediction. An indication of the prediction variability within the range of applicable operating speeds and at each angle, was obtained from the standard deviation of the SPL differences between the various data points and the spline fit used in the prediction. The degree of variability in the measured flyover data was determined from a comparison of BPF vs. angle curves for two similar flight conditions. These variabilities, as well as a comparison of the predicted and measured flyover levels, are discussed in the following paragraphs.

Comparisons were made between predicted and measured BPF and 2 BPF levels for each of the four flight conditions and plotted as a function of angle. Each plot consists of four curves, BPF_m (one sample of measured flyover levels), BPF_{ma} (average measured flyover levels), BPF_{PNI} (predicted NO ICS), and BPF_{PI} (predicted ICS). The bars on the BPF_{PI} plot indicate the degree of data variability at that particular angle due to the spline fit discussed above.

Plots of BPF and 2 BPF (predicted) vs. BPF and 2 BPF (measured) were useful in analyzing the ICS effectiveness by showing a bias one way or the other. A statistical evaluation of the differences between measured and predicted BPF tones was done for each flight condition and the results are shown on the plots of BPF predicted (BPF_p) vs BPF measured (BPF_m).

Approach 30^0 Flap

Plots of BPF vs. angle for approach, 30^0 flap, are shown in Figure 2. These plots show that the ICS prediction is closer to the measured data than the NO ICS prediction in the forward angles (30^0-60^0). In this angle range, the ICS prediction is 1-3 dB below the measured data and the NO ICS prediction is 5-7 dB high. Near overhead (70-95^0), the NO ICS prediction is within 1 dB of the measured BPF values, while the ICS predictioon is 3-5 dB below the measured data. In the aft angles (100-140^0), the measured data lies within the variability of the predicted ICS data, and the NO ICS prediction is 3-5 dB high.

The plots of 2 BPF vs. angle are shown in Figure 3. The curves in this figure show the ICS to have little effect on predicted 2 BPF levels. The measured and predicted values agree to within 2 dB for the angles 20^0 through 40^0. There is a peak in both predictions at 50^0 which is not seen in the flyover 2 BPF data. Near overhead and in the aft angles (70-140^0), the measured 2 BPF levels are 1-3 dB higher than both predictions.
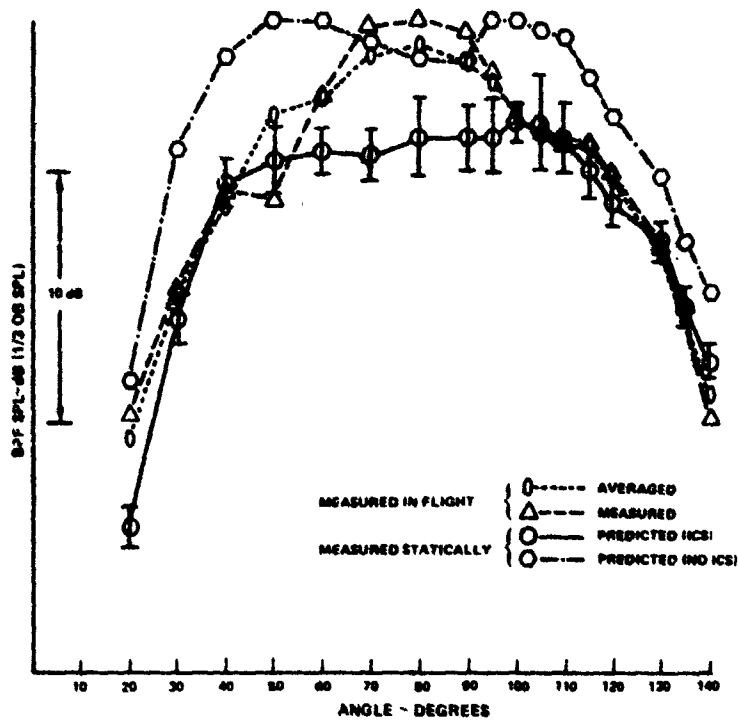
Figure 2 Comparison of Predicted Flight BPF Tone Levels (Based on Static Data) With Measured Flyover Tone Levels; Approach 30° Flap
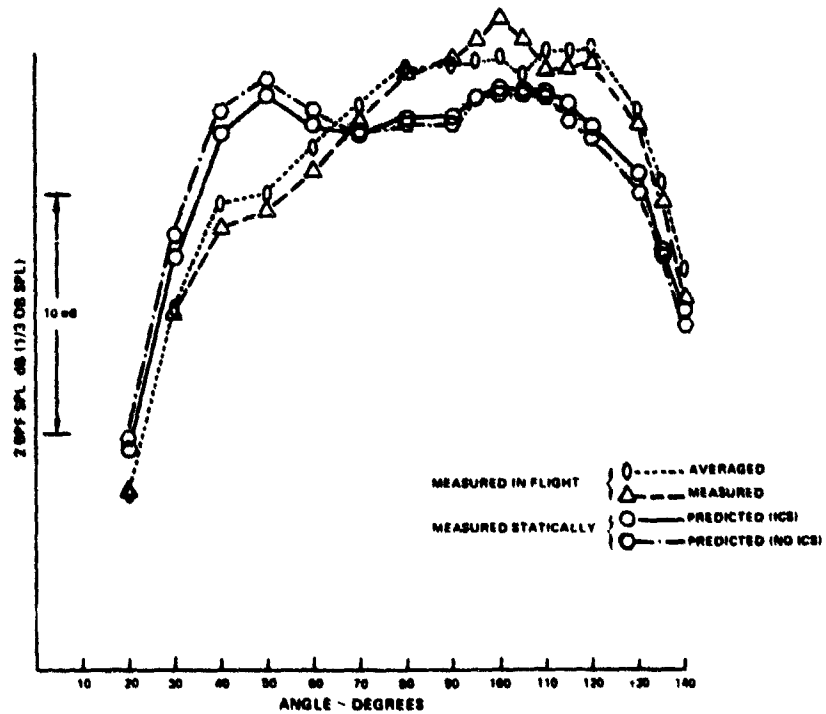

Figure 3 Comparison of Predicted Flight 2BPF Tone Levels (Based on Static Data) With Measured Flyover Tone Levels; Approach 30° Flap

14

Figure 4 shows a plot of BPF_{PNI} vs. BPF_{ma} for the NO ICS prediction. Each data point on this figure corresponds to a measured and predicted BPF level at a particular angle. The line denoting equality of the predicted and measured BPF is drawn on the plot as a reference. The data points on the plot are consistently above the line indicating an overprediction. A statistical assessment of how well the projected static data agreed with the flight data was performed by taking the average of $(BPF_{ma} - BPF_{PNI})$ for all angles since this average is a measure of how much error there is between the predicted and measured values. The standard deviation then provides a measure of the variability of this quantity about the mean. For the ideal case where $BPF_{ma} = BPF_{PNI}$ for every angle on Figure 3, then $BPF_{ma} - BPF_{PNI} = 0$, the mean of these quantities and the standard deviation would be zero. If the mean is negative, this implies an overprediction on the average. The mean, denoted by $(BPF_{ma} - BPF_{PNI})_a$, for the data of Figure 4 was found equal to -3.0 while the standard deviation was 1.7 dB.
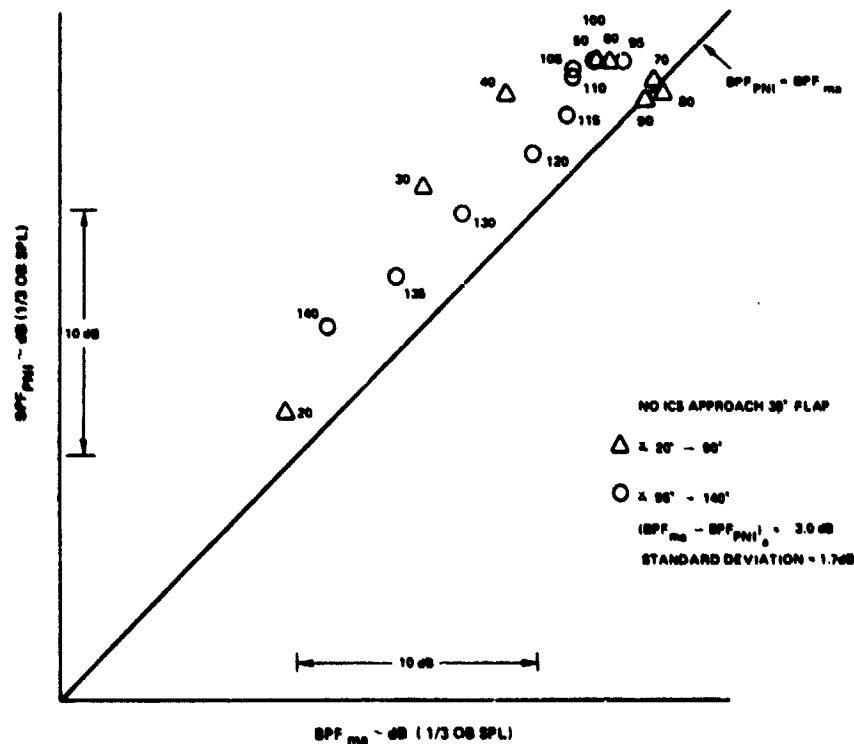
Figure 4   Predicted BPF (no ICS) Compared With Average of Flight Data; Approach 30° Flap

The BPF_{PI} vs. BPF_{ma} plot for the ICS prediction is shown in Figure 5. The data points in this figure are much closer to the $BPF_p = BPF_m$ line indicating an improved prediction. In this case $(BPF_{ma} - BPF_{PI})_a$ was found to be equal to 1.2 $\pm$1.6 dB, showing much better agreement of the prediction with the flyover data when static data from an ICS is used, with about the same scatter.
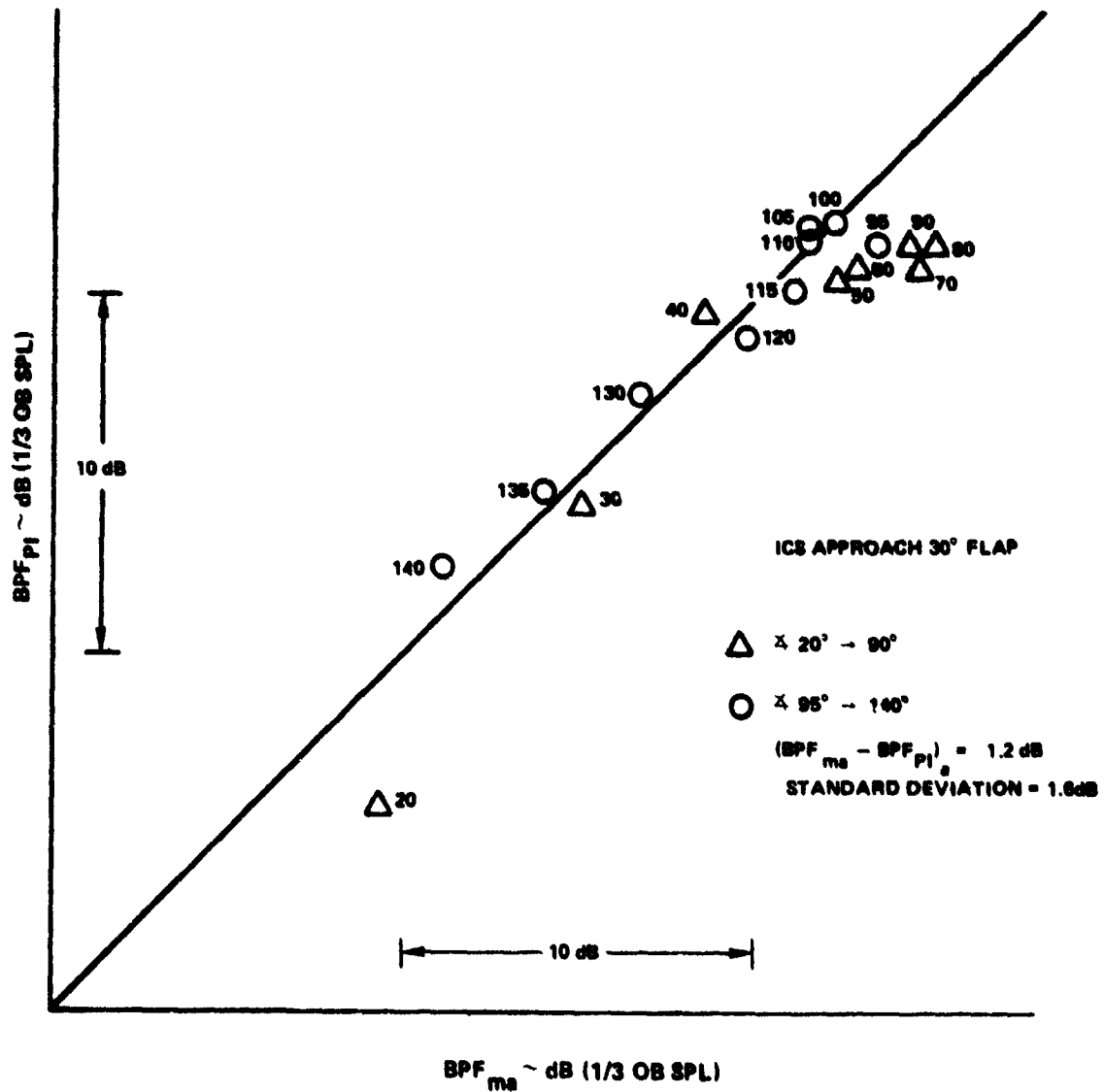

BPF$_{ma}$ ~ dB (1/3 OB SPL)

Figure 5   Predicted BPF (ICS) Compared With Average of Flight Data;
             Approach 30° Flap

16

Approach 25$^{\text{o}}$ Flap

Plots of BPF vs. angle for approach, 25$^{\text{o}}$ flap, are shown in Figure 6.
Measured BPF values are 3-7 dB below the no ICS prediction at all angles. The
ICS prediction is very close to the measured data, with the measured BPF
values falling within the range of variability of the prediction at most
angles. The BPF flight average vs. angle curve for an approach, 25$^{\text{o}}$ flap,
does not show the rise in BPF value at overhead which was shown for the
approach 30$^{\text{o}}$ flap case in Figure 2.

Plots of 2 BPF vs. angle are shown in Figure 7. As was the case for approach
30$^{\text{o}}$ flap, the ICS has little effect on 2 BPF levels. The 2 BPF prediction
shows a peak at 50$^{\text{o}}$ which was not evident in the measured data. This
characteristic was also evident in the approach 30$^{\text{o}}$ flap case. The measured
2 BPF curve peaks at 120$^{\text{o}}$, 3 dB above the prediction. At all angles greater
than 70$^{\text{o}}$ the predicted 2 BPF curves are 2-5 dB below the measured 2 BPF
values. In short, the 2 BPF vs. angle curves show little effect of the ICS
and are very similar for the two approach cases.

Figure 8 shows a plot of BPF_{PNI} vs. BPF_{ma} for the no ICS case. All of the
points on this plot, except 20$^{\text{o}}$, are well above the $BPF_m = BPF_p$ line,
indicating a consistent overprediction. $(BPF_{ma} - BPF_{PNI})_a$ was found to
be equal to -4.5 $\pm$1.4 dB, supporting this observation.

A plot of BPF_{PI} vs. BPF_m is shown in Figure 9 for the ICS case. The data
points on this plot are grouped around the $BPF_m = BPF_p$ line, showing an
underprediction in the smaller angles and an overprediction in the larger
angles. The proximity of the data points to the $BPF_m = BPF_p$ line is in-
dicated by $(BPF_{ma} - BPF_{PI})_a$ being equal to -0.1 $\pm$1.4 dB.

Figure 6 Comparison of Predicted Flyover BPF Tone Levels (Based on Static Data) With Measured Flyover Tone Levels; Approach 25° Flap
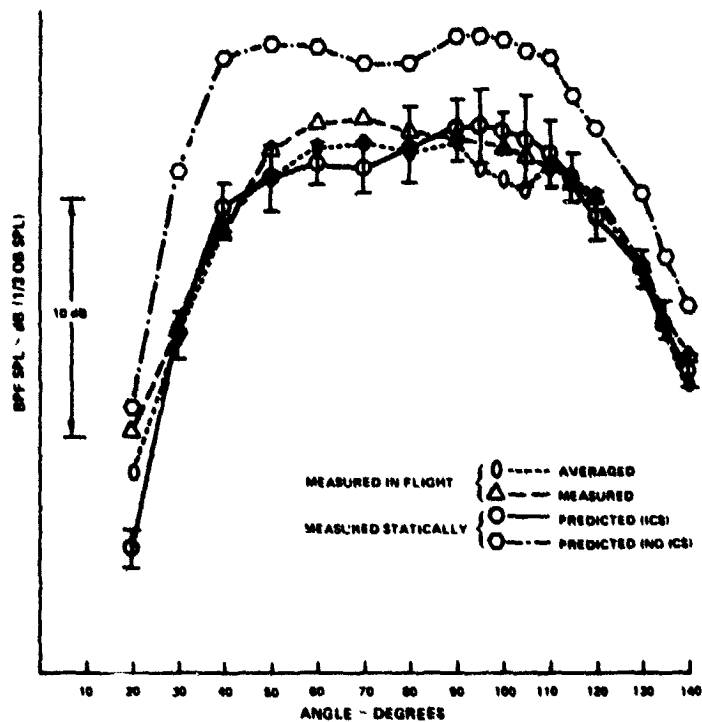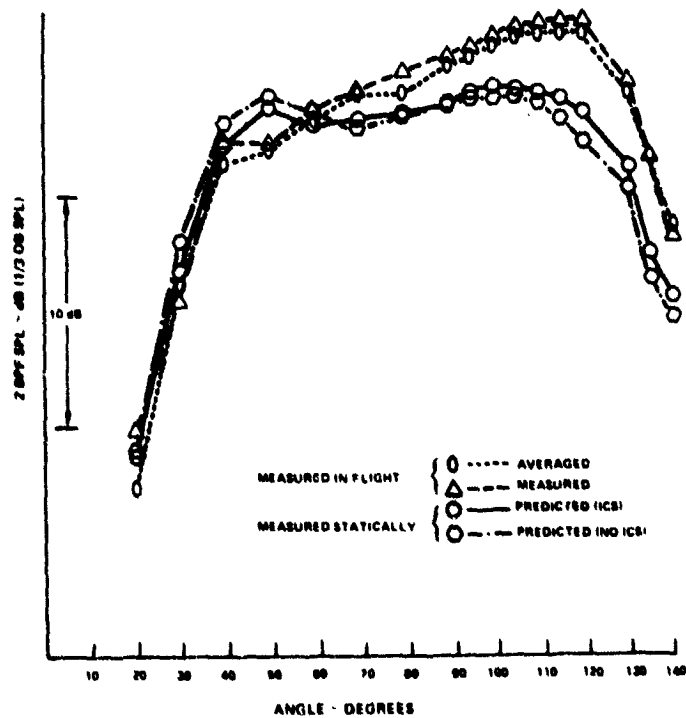

Figure 7 Comparison of Predicted Flight 2 BPF Tone Levels (Based on Static Data) With Measured Flyover Tone Levels; Approach 25° Flap
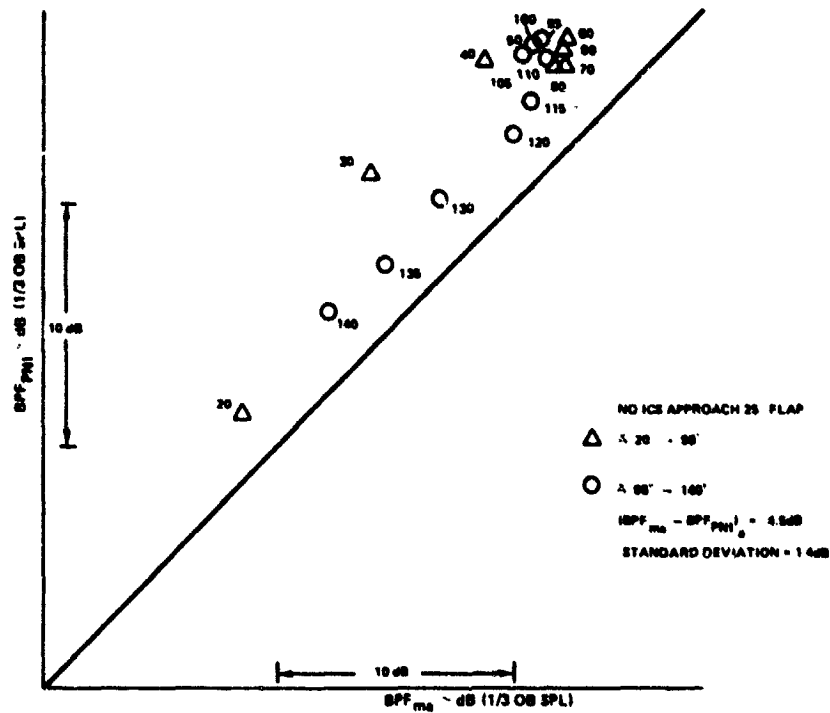
18

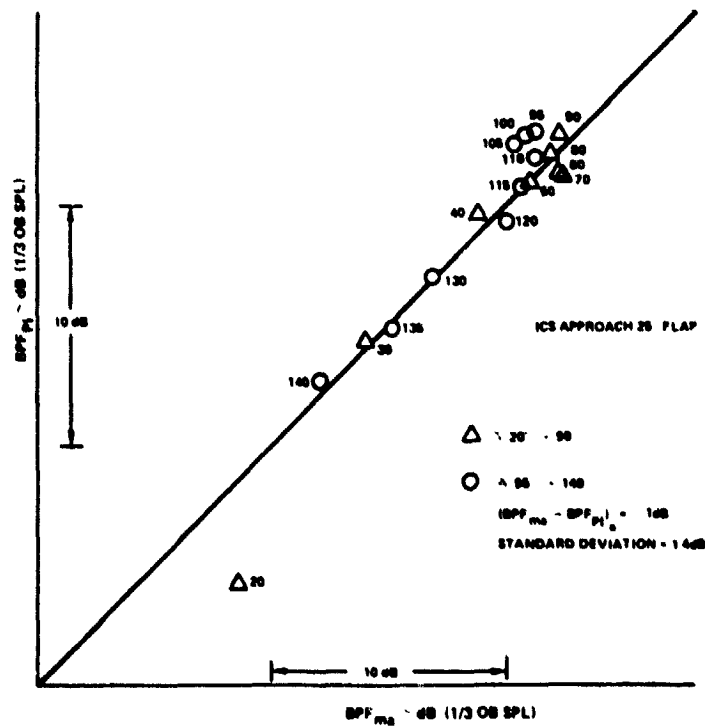Figure 8   Predicted BPF (no ICS) Compared With Average of Flight Data;
Approach 25° Flap

Figure 9   Predicted BPF (ICS) Compared With Average of Flight Data; Approach
25° Flap

19

Takeoff

Narrow band spectra showed that the SPL levels of the one third octave bands containing the BPF and 2 BPF tones were set by the tones and not the buzz saw harmonics contained in those one third octave bands. The plots of BPF vs. angle for takeoff are shown in Figure 10. These plots show the ICS prediction to be slightly better than the no ICS prediction in the forward angles. The ICS prediction in this region is 0-5 dB above the measured data as compared to a 3-5 dB overprediction from the no ICS data. Near overhead ($90-105^O$) the ICS predicted and measured BPF values are very close, with the measured data falling within the range of scatter of the predicted curve. In this region, the NO ICS prediction is 1-2 dB above the measured data. Through the aft angles (110°-140°) the no ICS prediction is 2-5 dB above the measured data and the ICS prediction is 1-5 dB above the measured data. It should be noted that measured and predicted BPF curves have similar shapes.

Two BPF vs. angle plots are contained in Figure 11. As was the case for approach, the ICS changes 2 BPF levels slightly. In the angles 40 to 60°, the no ICS prediction is 1-2 dB above the ICS prediction. The two prcJictions are essentially identical for the rest of the angles. The ICS prediction is approximately 8 dB above the measured 2 BPF values for the angles 50 to 70°. For all angles larger than 70°, predicted 2 BPF values are 1-4 dB above the measured data.

Figure 12 contains a plot of BPF_{PNI} vs. BPF_{ma} for the no ICS case. Most data points on this plot are well above the $BPF_m = BPF_p$ line, indicating an overprediction. A statistical evaluation showed $(BPF_{ma} - BPF_{PNI})_a$ to be equal to -3.2 ± 1.5 dB.

A plot of BPF_{PI} vs. BPF_{ma} for the ICS prediction is shown in Figure 13. Again all the data points are above $BPF_m = BPF_p$ curve indicating an over-prediction. The value of $(BPF_{ma} - BPF_{PI})_a$ for the ICS prediction was equal to -1.8 ± 2.3 dB, indicating an improvement over the no ICS prediction.

Figure 10   Comparison of Predicted Flight BPF Tone Levels (Based on Static Data) With Measured Flyover Tone Levels; Takeoff

Figure 11   Comparison of Predicted Flight 2 BPF Tone Levels (Based on Static Data) With Measured Flyover Tone Levels; Takeoff

21

Figure 12   Predicted BPF (no ICS) Compared With Average of Flight Data;
Takeoff

Figure 13   Predicted BPF (ICS) Compared With Average of Flight Data; Takeoff

22

Cutback

The BPF vs. angle plots are shown in Figure 14. In the forward angles, the biggest discrepancy between predicted and measured BPF values occurs between 30 and 60°. In this range, the no ICS prediction is 8-11 dB above the measured BPF values, and the ICS prediction is 3-7 dB above the measured values. In the range of angles 70 to 90° both predictions improve; the no ICS prediction is 1-2.5 dB above the measured data and the ICS predictions agree well with the measured BPF values. The measured data falls off faster than either of the two predictions in the aft angles (95-140°). In this region the no ICS prediction is 3-6 dB above the measured data, and the ICS prediction is 1-4 dB above the measured data.

Figure 15 contains 2 BFF vs. angle plots. These plots show that the effect of the ICS is small i∴ the forward angles (30 to 70°). In this region, both predictions are 5-12 dB above the measured data. For the angles (80-120°), the no ICS prediction is similar to the ICS prediction and approaches the measured data towards overhead. In the aft angles (130°-140ᶜ) the no ICS 2 BPF prediction is 2-6 dB below the measured 2 BPF values and the ICS prediction is closer, being 1-4 dB below the measured values.

Figure 16 shows a plot of BPF_{PNI} vs. BPF_m for the no ICS case. The data points for each angle are all above the $BPF_m = BPF_p$ line, indicating an overprediction. The value of $(BPF_m - BPF_{PNI})_a$ was calculated to be equal to -5.0 ±2.7 dB. Figure 17 shows similar plots for BPF_{PI} vs BPF_m, for the ICS case. Again overprediction is indicated, with the value of $(BPF_m - BPF_{PI})_a$ calculated to be - 2.6 ± 2.3 dB.
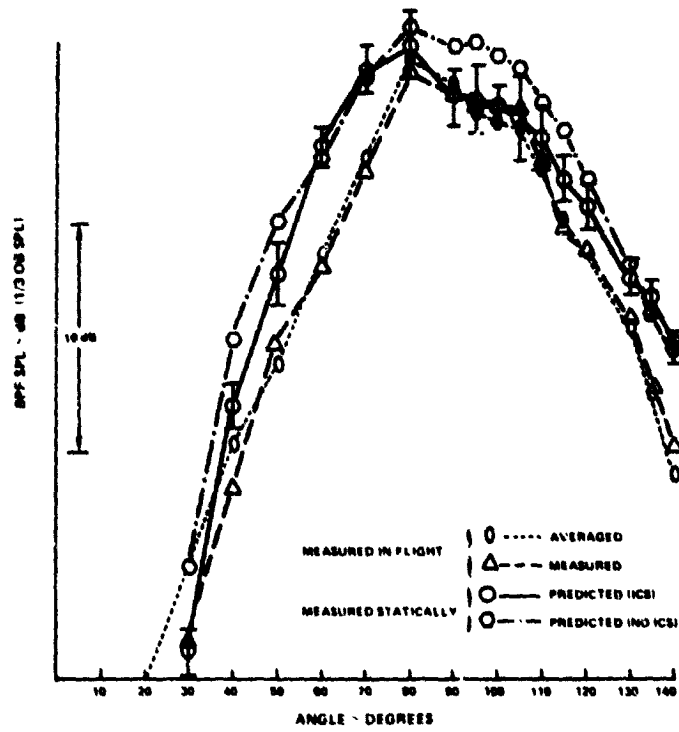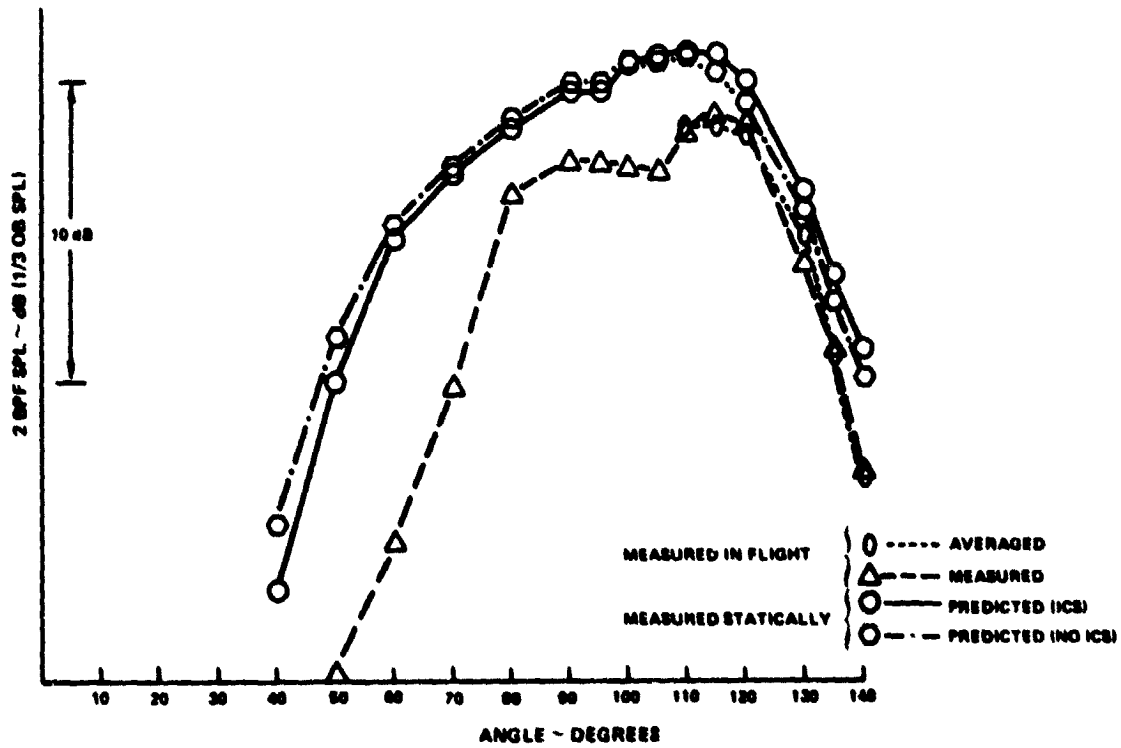
23

Figure 14 *Comparison of Predicted Flyover BPF Tone Levels (Based on Static Data) With Measured Flyover Tone Leve's; Cutback*

Figure 15 *Comparison of Predicted Flyover 2 BPF Tone Levels (Based on Static Data) With Measured Flyover Tone Levels; Cutback*
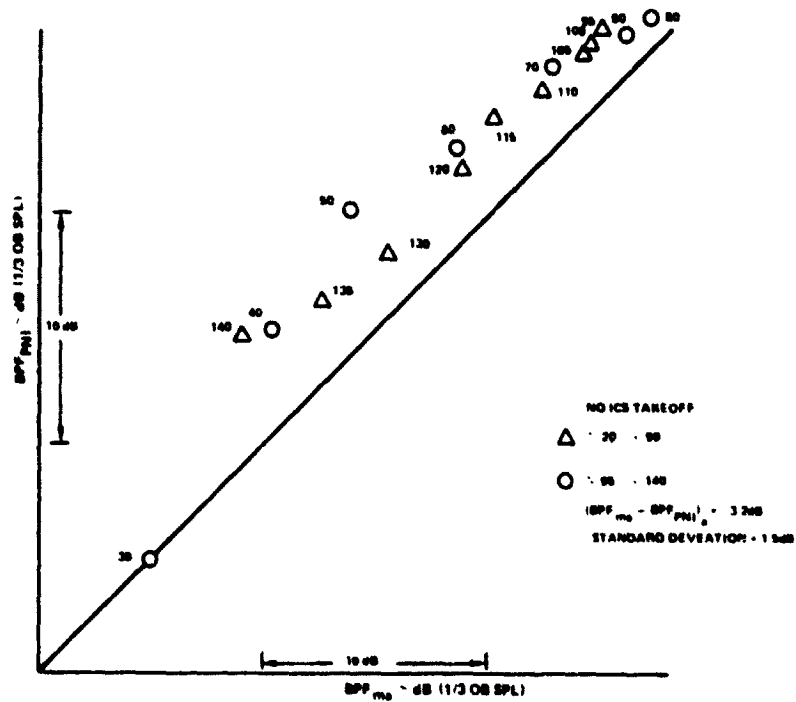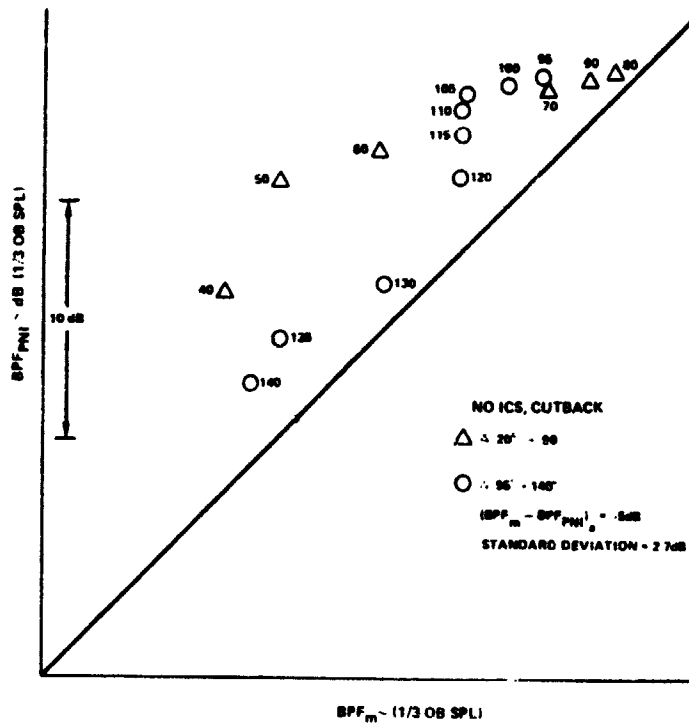
Figure 16   Predicted BPF (no ICS) Compared With Average Flight Data; Cutback
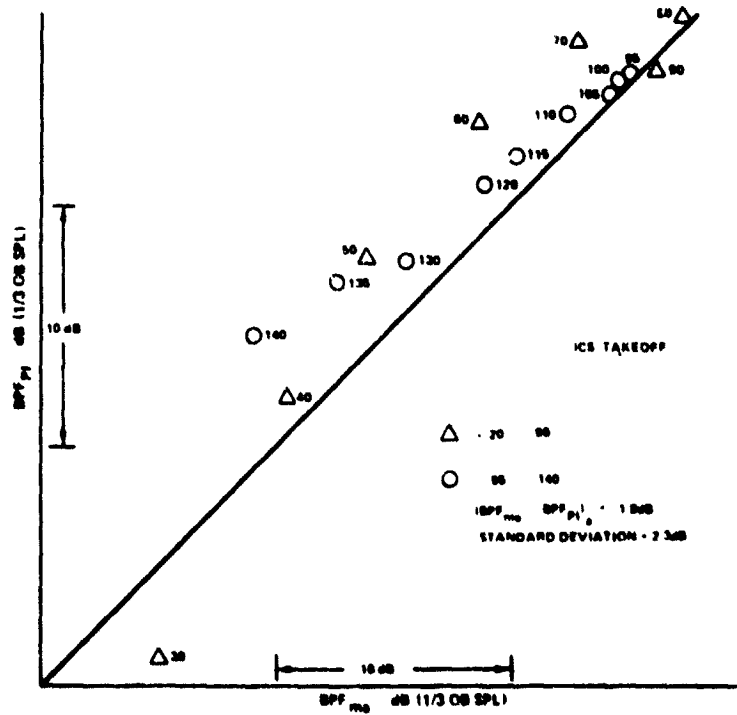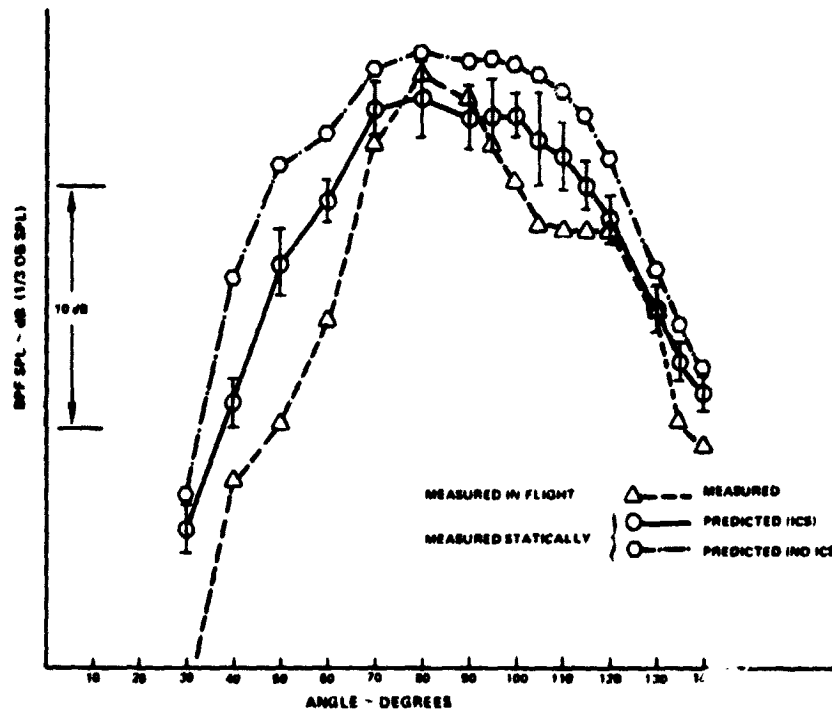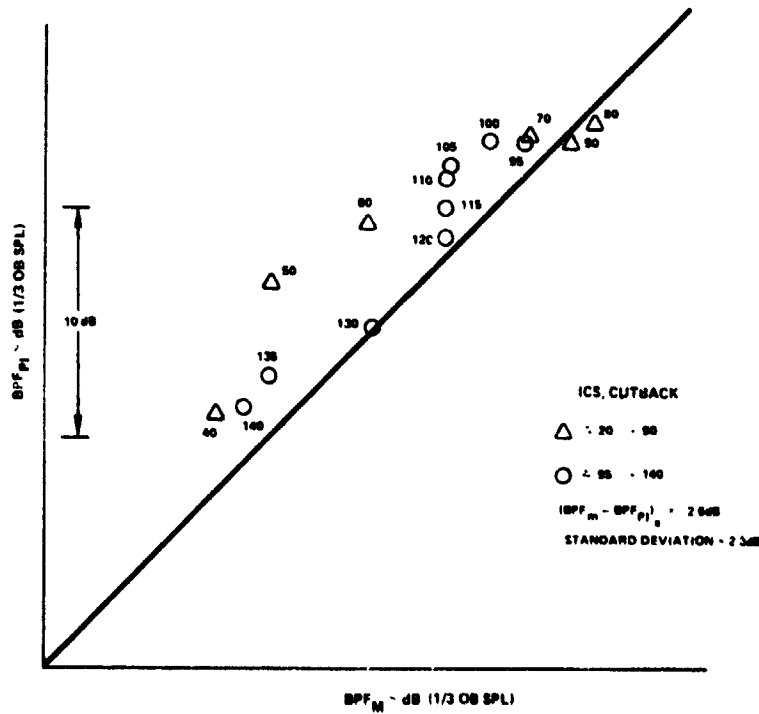

Figure 17   Predicted BPF (ICS) Compared With Average Flight Data; Cutback

Discussion of Data Variability

The variability in measured flyover data for BPF and 2BPF is shown by com-
paring average BPF and 2BPF levels (levels averaged between 2 similar runs and
shown in Figures 2, 3, 6, 7, 10 and 11) with BPF and 2BPF levels from a single
run . This comparison was done for all powers except cutback, where only one
set of flyover data was obtained. Because the averaging was limited to two
runs, these comparisons can provide only an indication of flyover data
variability. In those cases for which repeat flyover data was available, the
difference between the mean and the actual sample is in general less than 1.5
dB. Thus, the variability in the flyover data was small.

The variability in the measured static data relative to the spline fit curve
regressed through the data is represented by the bars through the predicted
BPF points (see Figures 2, 6, and 10). The variability is more substantial
than for the flyover data, peaking at a value of ± 1.6 dB (representing a
difference of 3.2 dB) near the overhead angles and decreasing to ± 0.5 dB at
20^0 and 40^0. Because of this variability in the data the assessment of the
static test procedures can only be made to within about ± 1.6 dB.

It should be noted that the standard deviation defined previously is related
to the differences between the predictions based on the mean of the static
data and the mean of the flyover data, and is not directly related to the
variability in the data (i.e. even if data variability for both data sets is
zero, there could be a difference between the predicted and measured values).
This standard deviation ranged from 1.4 to 3.0 dB. If this is compared with
the somewhat smaller variability in the data, which is typically ± 1.6 dB or
less, the conclusion can be drawn that the differences between the predictions
based on the mean of the static data and the mean of the measured flyover data
are statistically significant and are a measure of the accuracy that results
if static data is used to predict flight.

26

Discussion of ICS Effectiveness

In each of the conditions examined, a statistical analysis of the measured
flight mean BPF tone minus the predicted value based on the averaged measured
static data projected to flight was carried out to indicate if:

a) Use of an ICS improved prediction accuracy.

b) Use of an ICS reduced the scatter in the difference between measured and
   predicted noise levels.

Figure 18 shows a table of the results of the statistical analysis. Considering
first the analyses for each power setting, it is clear that differences be-
tween the predicted and measured data are reduced with the use of an ICS. In
fact, if differences are averaged for all power settings and angles it can be
seen that without an ICS, BPF is predicted 3.9 dB higher than measured. Use of
an ICS results in only a 0.8 dB overprediction, a significant improvement. If
the standard deviations in Figure 18 are studied, it can be seen that the use
of an ICS does not significantly alter the scatter of the predictions relative
to the data.

FLIGHT CONDITION	NO ICS $(BPF_{ma} - BPF_{PNI})_a$ dB	WITH ICS $(BPF_{ma} - BPF_{PI})_a$ dB
APPROACH 30° FLAP	-3 ±1.7	1.2 ±1.6 dB
APPROACH 25° FLAP	-4.5 ±1.4	-0.1 ±1.4
TAKEOFF	-3.2 ±1.5	-1.8 ±2.3
CUTBACK	-5.0 ±2.7	-2.6 ±2.3
AVERAGE OVER ALL ANGLES AND POWER SETTINGS	-3.9 ±1.8	-0.8 ±1.9

*Figure 18   Comparison of Averaged Measured Minus Predicted Values of BPF Tone
for Cases With and Without an ICS.*

Based on the BPF comparisons discussed above, data obtained statically from a
JT9D engine with the PWA ICS installed and projected to flight, on the average,
gave predictions that were 0.8 $\pm$1.9 dB higher than measured. Similar data
projections without an ICS, gave predictions that were 3.9 $\pm$1.8 dB higher than
measured. Since the variability in both sets of measured data is on the order
of $\pm$1.6 dB, the agreement between the ICS prediction and the measured data on
the average, is probably as close as can be expected.

Review of the 2 BPF static data shows that the effect of the ICS on the
radiated sound field is small. Differences in comparisons of predicted with
flight for 2 BPF should then be caused primarily by errors in the corrections
used for projecting static data to flight or data scatter. For the two
approach and cutback conditions the predictions are higher than the measured
for the forward angles and lower for the aft angles. For the takeoff case, the
predictions are generally greater than the measured for all angles. These
comparisons suggest that a possible reason for the discrepancy is that the
convective amplification correction may be too high in the forward quadrant
and too low in the aft. A reduction in exponent from the value of four
commonly used would result in improved agreement between the predictions and
the measured data. This observation is based on the limited data comparison
contained herein, and is not conclusive. The corrections used to project
static data to flight are consistent with the current state of the art. It is
difficult to pinpoint errors in any one of these corrections (i.e. convective
amplification) as being totally responsible for the observed differences
between predicted and measured flyover data. Other corrections that could have
errors in them include, long distance propagation in the atmosphere, i.e.,
sound is scattered by turbulence in the atmosphere, an effect which is
currently not included in the corrections. Additionally, extra ground attenua-
tion is presently an empirical correction whose physical origin has yet to be
defined. Non-linear sound propagation effects become significant at large
propagation distances, an effect not included in the corrections. Refraction
of sound by velocity and temperature gradients in the atmosphere are not
included in the predictions, although they can be partially included by use of
a layered atmosphere. Reflection and diffraction caused by an aircrafts'
wings and fuselage are not included in the corrections. In view of these
possible omissions, it is recommended that these corrections be further
assessed and improved as required.

28

Further evaluations of the PWA ICS and evaluation of the Boeing ICS are reported in Reference 4. Comparisons are made at the spectral level for three angles using data from both ICS's for approach and takeoff power, (see Figures 21, 22, 23, 24 of Reference 4). As is evident, there is very good agreement between the flyover data and the static data projected to flight. In addition, since FAA noise certification procedures require assessment of noise levels in terms of Perceived Noise Levels (PNL), PNL time histories are also compared in Figure 25 of Reference 4. Again very good agreement results.

From the above discussions, the following conclusions can be drawn.

o   The use of an ICS in static fan noise testing of high bypass ratio (HBPR) engines, combined with a comprehensive static-to-flight projection technique, provides an improved method for obtaining predictions of flight fan noise levels using static data.

o   The ICS effectiveness has been demonstrated for the JT9D-7 engine type. Other HBPR engines with different fan noise characteristics may show different acoustic results, and further evaluation using other engine data, such as that from the JT15D, would be beneficial in further verifying ICS effectiveness.

4.5   Work Plan For Further Evaluation of the Procedures Report (Phase III, Task E)

During the contract period, support was provided to NASA to help in planning their JT15D test programs and interpreting the resulting data as well as helping in coordination of the contract. As part of this support, periodic reviews were held with NASA Langley and Lewis describing results of Pratt & Whitney Aircraft studies and making suggestions for NASA's programs based on experience in the Pratt & Whitney Aircraft/Boeing Joint Noise Program. In addition, written comments on NASA's JT15D installation on the OV-1 were also provided. This provided a familiarity with NASA's programs, which when coupled to the results of this contract and the results of the Pratt & Whitney Aircraft/Boeing joint program, have indicated the need for further work,

29

supplemental to NASA's current plans. A work plan defining the various elements of this further work has been defined and is included as Appendix IV of this report.

The elements suggested as requiring further work are outlined below:

I. ICS's
   1. Assess NASA ICS designs using Procedures Report.
   2. Assess Procedures Report by projecting static data to flight and comparing to JT15D flight data and update Procedures Report.
   3. Define additional test programs required based on results of 1) & 2) above.

II. Ames Tunnel
   4. Define corrections required to project Ames tunnel data to flight.
   5. Assess effectiveness of Ames tunnel as a simulation of flight.

III. Rig Testing
   6. Assess effectiveness of rig testing in anechoic chamber with ICS as simulation of flight.

IV. Inlet Boundary Layer Simulation
   7. Assess importance of this simulation.
   8. Develop inlet design and boundary layer control methods if shown to be necessary in Step 7.

V. Misc.
   9. Provide technical assistance to support NASA in JT15D flyover program.
   10. Conduct investigation to define starting conditions for inflow distortions generated by the flow over the ground plane and stand structure.

30

5.0 RESULTS, CONCLUSIONS AND RECOMMENDATIONS

Major conclusions and recommendations from Phase I and Phase II, as they impact the development of the procedures report, are listed below along with the major conclusions and recommendations from Phase III. Inclusive lists of conclusions and recommendations from Phase I and Phase II are given in References 1, 2, and 3.

5.1 Results and Conclusions

Phase I

1. Based on a literature search, an atmospheric turbulence model has been selected that predicts turbulence intensities, integral scales and spectra as a function of the altitude above the ground, the mean wind velocity, the surface roughness and atmospheric stability.

2. The difference in fan tone sound power at BPF due to ingested atmospheric turbulence between typical static test conditions and typical landing approach conditions is on the order of 30 dB. Based on this difference, it is concluded that fan noise due to ingested atmospheric turbulence is negligible in landing approach conditions for the currently used high bypass ratio engines.

3. Fan tone noise due to convected turbulence is dominated by the distortion elements within a small range of transverse scales. For typical turbulence energy distributions this range covers about one decade and is centered around a transverse scale in the order of 30% of the rotor blade spacing at the blade tip. For a given turbulence variance, maximum sound power levels are achieved at transverse integral scales in the order of 25% of the rotor blade spacing at the blade tip. For a JT9D fan this is about 4.1 cm and for the JT15D fan it is about 1.3 cm.

4. Duct, inlet and fuselage pressure variations, measured during flyover tests of a 747 equipped with JT9D engines, indicate that there is no obvious correlation between inlet angle of attack changes and changes in broadband noise as well as narrowband noise at the first three harmonics of the fan blade passing frequency.

Phase II

5. Using analytical models and test data on the effects of contraction and screening on steady and unsteady distortions, an ICS design system was developed. Honeycomb was found to be particularly effective in removing transverse velocity distortions.

6. ICS propagation effects caused by corners and structure such as those in the PWA ICS were found to be controllable to levels within the repeatability of measured far-field acoustic static data. The following techniques should be used to minimize transmission effects; design which minimizes corners, sharp changes in ICS radius and support structure other than the honeycomb/perforated plate covering; controlled speed variations of the order of 0.5% during the time period acoustic data is obtained.

7. Analysis of Blade Mounted Transducer Data, obtained without an ICS, showed that significant amounts of inflow distortion were generated by the flow over the ground plane and stand structure.

8. The ICS design system velocities predicted for the ICS case were 2-4 orders of magnitude less than the velocities inferred from BMT data. This indicated that the BMT signal was set by phenomena other than inflow distortion. Velocities calculated from hot film data were in much closer agreement with the design system predictions.

32

Phase III

9. An Interim Procedures Report was developed that gives step by step instructions for the design of an ICS, the conduct of the static test program using the ICS mounted on an engine and the projection of the resulting static data to flight.

10. Assessment of the Procedures Report using flyover data from a 747 equipped with JT9D engines and static data from tests of a JT9D engine operated with and without an ICS showed that use of data obtained from the PWA ICS design projected to flight improved the agreement between flyover data and static data projected to flight by 3.1 dB for the blade passage frequency tone. A similar assessment resulted when data obtained with the Boeing ICS was used.

5.2 Recommendations (All Phases)

1. Assess and improve Interim Procedures Report using NASA JT15D static data obtained with an ICS and flyover data to be obtained during flight tests with a JT15D engine mounted on the OV-1.

2. Assess the importance of and develop a system to provide inlet designs for use in static testing that properly represent the aerodynamic properties and the acoustic radiation characteristics of flight inlets operated in flight.

3. Assess the validity of testing in the Ames Wind Tunnel by developing and applying corrections for projecting wind tunnel data to flight and by comparing with JT15D flyover data to be obtained during flight tests of the OV-1.

33

4. Assess the validity of testing fan rigs in anechoic chambers with ICS's by projecting data from such tests conducted with the JT15D engine to flight and comparing with the flyover data to be obtained during flight tests of the OV-1.

5. Conduct analytical and experimental studies to define the distortion velocity field induced by flow over the ground plane and engine test stand structure.

6. Investigate further the need to:

    a) Account for the three-dimensional noise field of a fan during static testing.

    b) Obtain test data with variable fan speed.

    c) Use different nozzle areas for static testing than used in flight or generate an appropriate set of corrections to properly account for flight ram effects during static testing.

7. Further assess, and improve as required, the static to flight projection methodology.

REFERENCES

1. Ganz, U. W. "Analytical Investigation of Fan Tone Noise Due to Ingested Atmospheric Turbulence" Phase I Final Report, NASA Contract No. NAS1-15085, NASA CR 3302, August 1980.

2. Gedge, M. R. "Analytical Models for Use in Fan Inflow Control Structure Design", Phase II Interim Report, NASA Contract No. NAS1-15085, NASA CR 159189, May 1980.

3. Gedge, M. R. "A Design Procedure For Fan Inflow Control Structures" Phase II Final Report, NASA Contract No. NAS1-15085, NASA CR 165625, Sept 1980.

4. Atvars, Y. and Rogers, D. F. "The Development of Inflow Control Devices for Improved Simulation of Flight Noise Levels During Static Testing of a HBPR Turbofan Engine" AIAA Paper 80-1024, June, 1980.

APPENDIX I

INTERIM PROCEDURES REPORT

PROCEDURES FOR THE DESIGN OF INFLOW CONTROL STRUCTURES, STATIC
TEST TECHNIQUES AND PROJECTION OF STATIC DATA TO FLIGHT

1.0 INTRODUCTION

A difference exists between fan flyover noise predictions, based on static
engine test data and measurements made during aircraft flyovers. This differ-
ence in fan noise, which is observed primarily in the blade passing frequency
tones, is ascribed to distortions in the fan inflow field that exist during
static testing but not during flight. The inflow distortions present stat:
cally, but not in flight, include:

i) Steady and quasi steady distortion induced by flow over stand
structure and the ground plane.

ii) Turbulence induced by flow over stand structure.

iii) Distortion of atmospheric turbulence caused by the large con-
traction of the mean flow that occurs during static testing.

Effective suppression of these distortions can be provided by use of hemisphe-
rically shaped Inflow Control Structures (ICS), placed upstream of the fan,
that are constructed of honeycomb and perforated plate. An example of an
Inflow Control Structure, constructed by PWA and mounted on a JT9D engine, is
shown in Figure 1A. This design is an octagonal (flat panel) approximation of
a Hemisphere of 24 foot equivalent diameter. The panels consisted of about 50%
open area perforated plate face sheets with $l/d = 8$ honeycomb backing. A
second generation Inflow Control Structure built by Boeing and also used on a
JT9D engine is shown in Figure 1B. Both of these Inflow Control Structures
have been shown to be effective in reducing inflow distortion generated noise
to levels comparable with those measured in flight (see References 1, 2 and 3).
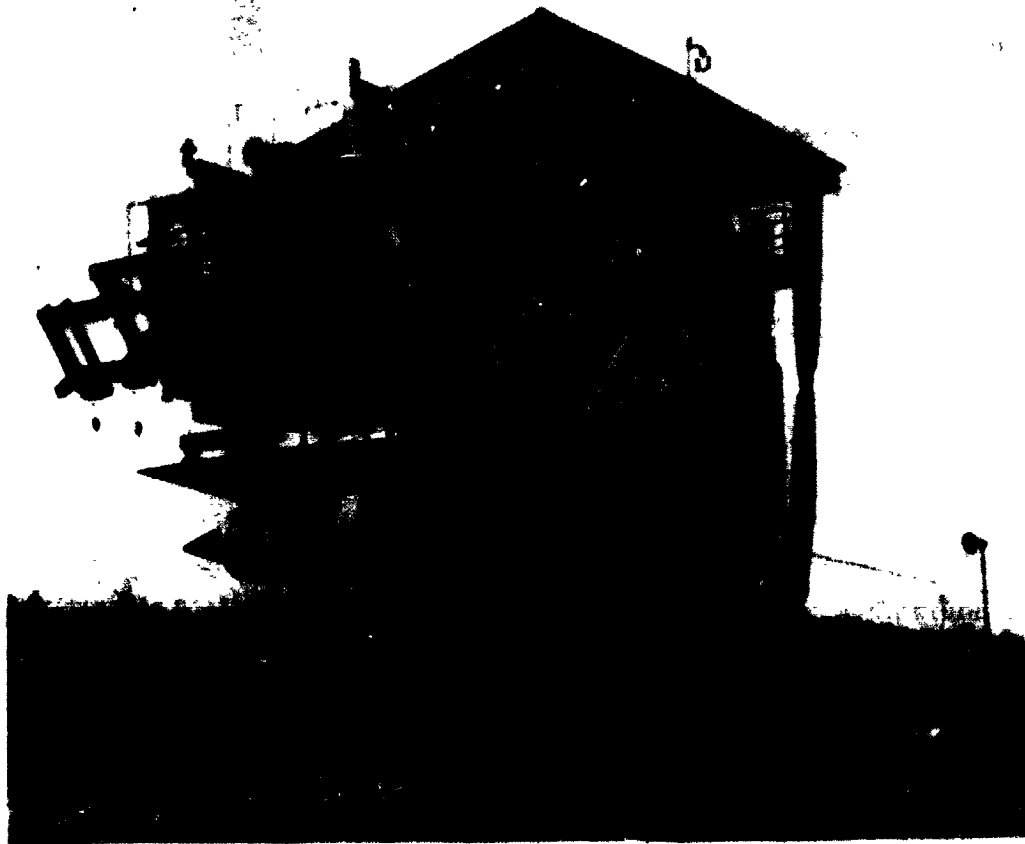
Figure 1A   Pratt & Whitney Aircraft Inflow Control Structure Mounted on JT9D
Engine
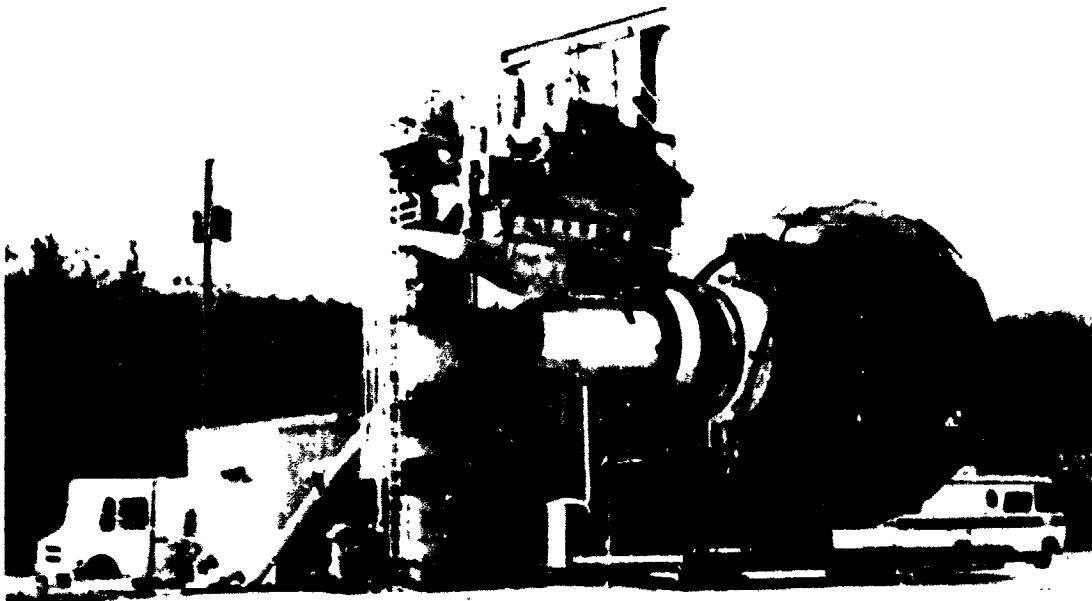
Figure 1B   Boeing Inflow Control Structure Mounted on JT9D Engine

The purpose of this interim procedures report is to provide step by step
instructions for:

> i) Designing an Inflow Control Structure for pplication to a
> specified engine.

> ii) Obtaining static test data with the Inflow Control Structure
> installed.

> iii) Projecting the static data to flight.

This procedures manual has been formulated using results from NASA Contract
NAS1-15085, "Forward Speed Effects on Fan Noise" (see References 3-6), and
from a Boeing/PWA joint program (See References 1 and 2), for the development
of static testing techniques.

The procedures manual is divided into the following sections:

> i)   Inflow Control Structure Design System

> ii)   Static Testing an i Data Recording and Analysis Procedures

> iii) Projection of Static Data to Flight

2.0   INFLOW CONTROL STRUCTURE DESIGN SYSTEM

Development of the system presented below for the design of Inflow Control
Structures is described in detail in Reference 6. Only the step by step proce-
dure is given here. Two design procedures are given, one that results in an
Inflow Control Structure design for suppression of turbulence to calculated
inflight turbulence levels and the other that results in a design for suppres-
sion of steady distortions to calculated inflight turbulence levels. The most
conservative design is then selected for construction. Note that Honeycomb is

38

used to remove primarily the azimuthal velocity components of inflow distortion whereas perforated plate reduces predominantly the streamwise velocity component of the inflow distortion.

2.1 General Information

1. Determine inlet velocity at lowest operating condition - U_O

2. Determine maximum ambient wind velocity in test window - U_A

3. Compute design speed at Inflow Control Structure - U_{ICS}
$$U_{ICS} = 1.5 \ U_A$$

4. Determine inlet radius - R_O

5. Compute nominal radius of Inflow Control Structure - R_{ICS}
$$R_{ICS} = R_O \ \sqrt{\frac{U_O}{2U_{ICS}}}$$

6. Determine fan rotor blade number - B

7. Compute minimum sensitive transverse scale - λ_{min}
$$\lambda_{min} = \frac{\pi R_O}{5B}$$

8. Compute final contraction ratio (Inflow Control Structure to inlet) - ℓ_{1F}
$$\ell_{1F} = \frac{U_O}{U_{1CS}}$$

[Note: Initial contraction ratio, from atmosphere to Inflow Control Structure, ℓ_{1I}, is equal to 1.5 by design]

9. Compute minimum sensitive transverse scale at Inflow Control Structure - $\left(\lambda_{min}\right)_{ICS}$

$$\left(\lambda_{min}\right)_{ICS} = \ell_{1F}^{1/2} \ \lambda_{min}$$

39

10. Compute characteristic detail dimension of Inflow Control Structure
    material - d_{ICS} (e.g. Honeycomb cell size)

$$d_{ICS} = o\left[\frac{(\lambda_{min})_{ICS}}{10}\right]$$

11. Compute Reynolds Number of honeycomb cell - Re

$$Re = \left[\frac{U_{ICS}\,d_{ICS}}{\nu}\right]$$

2.2 Atmospheric Turbulence Design

12. Determine engine height - z, roughness scale z_o ; (See Figure 2)
    static reference height (engine height) z_{REF} , static reference wind
    speed (max. wind speed in test window, Figure 3)U_{REF}.

13. Compute RMS value of turbulent velocity in capture stream tube during
    static operation -

$$\sqrt{\overline{u_{AS}^2}}$$

$$\sqrt{\overline{u_{AS}^2}} = \frac{.464\ R_o^{1/3}\ U_{REF}^{5/6}\ U_o^{1/6}\ z^{-1/3}}{\left(\ln\frac{z}{z_o}\right)^{1/6}\left(\ln\frac{z_{REF}}{z_o}\right)^{5/6}}$$

14. Compute static contraction ratio - ℓ_{1S}

$$\ell_{1S} = \frac{U_o}{\overline{U}_A}$$

15. Compute characteristic length scale of turbulence in capture stream-
    tube during static operation - L_{AS}

$$L_{AS} = .355\ R_o\ \ell_{1S}^{1/2}$$

TERRAIN DESCRIPTION OF AREA WITHIN SEVERAL KILOMETERS UPWIND OF SITE
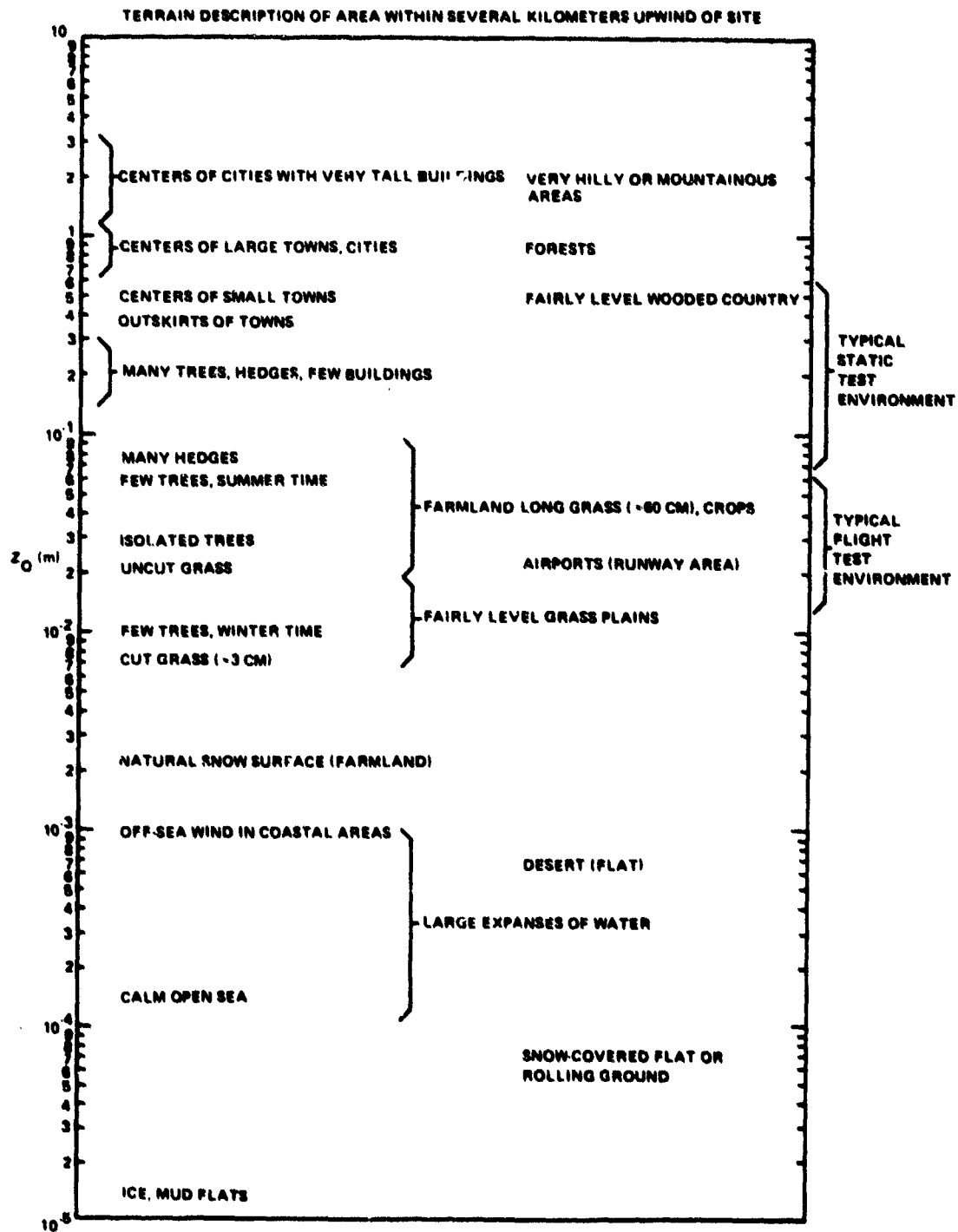
Figure 2   Values for Surface Roughness Scale z_0 (Ref. 18)
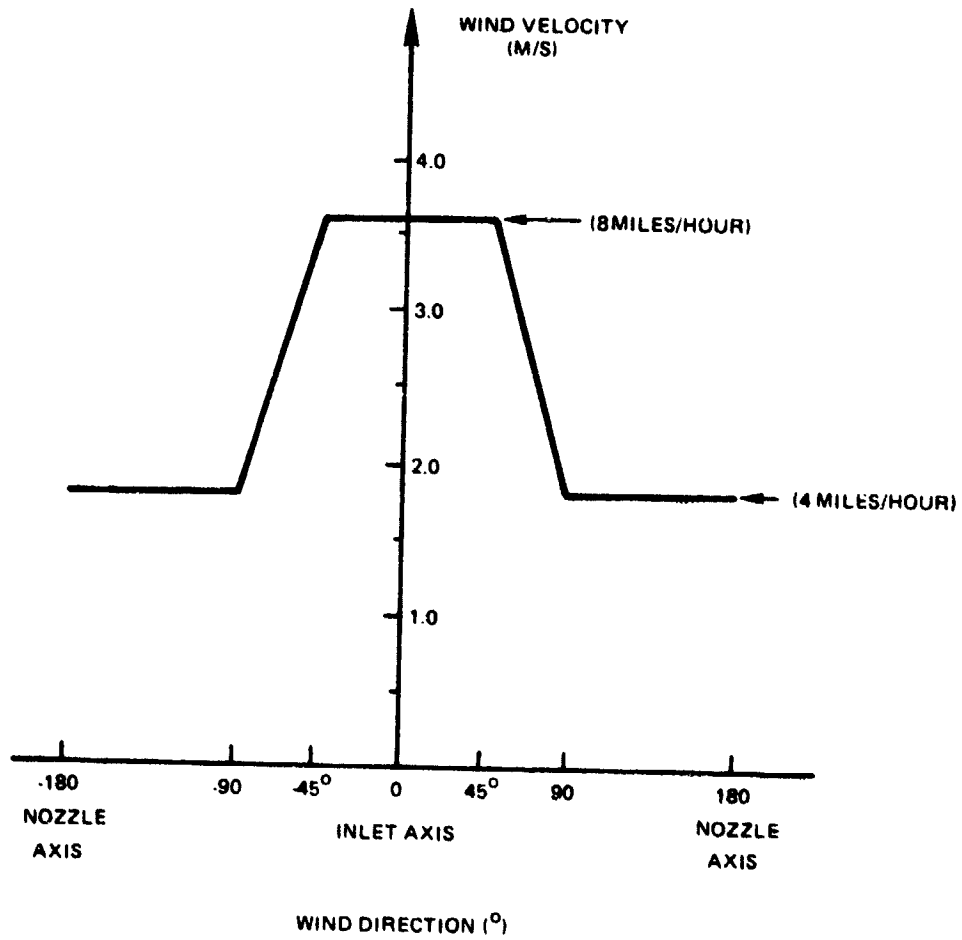
Figure 3   Typical Wind Limit Used in Static Fan Noise Tests

42

16. Determine, for flight operation, engine height z, roughness scale z_O (Figure 2), flight reference height $-z_{REF}$, flight reference wind speed $-U_{REF}$

17. Compute RMS value of turbulent velocity in capture stream tube in flight $-$

$$\sqrt{\overline{u_{AF}^2}}$$

$$\sqrt{\overline{u_{AF}^2}} = \frac{.464 \; R_O^{1/3} \; U_{REF} \; z^{-1/3}}{\left(\ln \frac{z}{z_O} \right)^{1/6} \left(\ln \frac{z_{REF}}{z_O} \right)^{5/6}}$$

18. Compute characteristic length scale of turbulence in capture stream-tube in flight $- L_{AF}$

$$L_{AF} = .355 \; R_O$$

19. Compute limits of sensitive wavenumber ranges $- k_1^*$, k_{2U}, k_{2L} k_{3U}, k_{3L}

$$k_1^* = \frac{B}{R_O} \;, \quad k_{2U} = k_{3U} = \frac{10B}{R_O} \;, \quad k_{2L} = k_{3L} = \frac{B}{2R_O}.$$

20. Compute in flight turbulence field characteristics $- N_F$, γ_F

$$N_F = \frac{2 \; \overline{u_{AF}^2}}{\pi^2 \; L_{AF}} \;, \quad \gamma_F = \frac{1}{L_{AF}}$$

21. Determine blade relative inflow angle at tip $- \gamma'$

22. Compute characteristic length scale of turbulence behind Inflow Control Structure - L_{ICS}

$$L_{ICS} = \frac{4}{3} \frac{L_{AS}}{\ell_{1I}^{1/2}} \qquad \text{if} > 1$$

$$= L_{AS} \qquad \text{Otherwise}$$

23. Compute the parameters p and s

$$p = \frac{k_{2L}^2 \ L_{ICS}^2}{\ell_{1F}} \qquad s = p + 1$$

24. Compute maximum value of flow angle ratio product - $\alpha_P \ \alpha_H$

$$\alpha_P \ \alpha_H = \left[\frac{32\pi \ N_F \ L_{AS}}{\ell_{1F} \ \ell_{1I}^{1/2} \ \overline{u_{AS}^2}} \cdot \frac{s \left(k_{3U} - k_{3L} \right) k_1^*}{\left\{ 4 \left(k_{2L}^2 + \gamma_F^2 \right) + \left(k_{3U} + k_{3L} \right)^2 \right\}^3} \cdot \right.$$

$$\left. \frac{\left(4k_{2L}^2 \ \sin^2 \gamma' + \left[k_{3U} + k_{3L} \right]^2 \right)}{\left\{ 1 + \frac{p}{2} + \frac{s\sqrt{p}}{4} \left[\sin^{-1}\left(1 - \frac{2}{s} \right) - \frac{\pi}{2} \right] \right\}} \right]^{1/2}$$

25. Solve the equation for perforated plate (gauze) flow angle ratio - α_P

$$\frac{2\alpha_P^3 + \alpha_P^2 - 1.21 \ \alpha_P}{\alpha_P^3 + 1.21} = .866 \ \alpha_P \ \alpha_H \ \ell_{1I}^{2/3}$$

$$\left\{ \frac{\alpha_P + \alpha_P \ \alpha_H - .201 \ Re^{-1/4} \ \alpha_P \left[\ell n \ \alpha_P \ \alpha_H - \ell n \ \alpha_P \right]}{\alpha_P + \alpha_P \ \alpha_H \left(1 + .201 \ Re^{-1/4} \left[\ell n \ \alpha_P \ \alpha_H - \ell n \ \alpha_P \right] \right)} \right\}$$

44

26. Compute resistance of perforated plate (gauze) - K_P

$$K_P = 1.21 \, \alpha_P^{-2} - 1$$

27. Compute flow angle ratio of honeycomb - α_H

$$\alpha_H = \frac{\alpha_P \, \alpha_H}{\alpha_P}$$

28. Compute resistance of honeycomb - K_H

$$K_H = - \, .201 \; Re^{-1/4} \, \ell n \, \alpha_H$$

2.3 Steady Distortion Design

29. Determine maximum azimuthal velocity in vortex - U_{2A}

30. Compute maximum value of flow angle ratio product - $\alpha_P \, \alpha_H$

$$\alpha_P \, \alpha_H = \frac{\sqrt{\overline{u_{AF}^2}}}{U_{2A}}$$

31. Determine maximum pre-contraction streamwise velocity deficit - ΔU_{1A}

32. Solve the equation for the perforated plate (gauze) flow angle ratio - α_P

$$\frac{2\alpha_P^3 + \alpha_P^2 - 1.21 \, \alpha_P}{\alpha_P^3 + 1.21} = \frac{\sqrt{\overline{u_{AF}^2}}}{\Delta U_{1A}} \, \ell_{1S}$$

$$\left\{ \frac{\alpha_P + \alpha_P \, \alpha_H - .201 \; Re^{-1/4} \, \alpha_P \left[\ell n \, \alpha_P \, \alpha_H - \ell n \, \alpha_P \right]}{\alpha_P + \alpha_P \, \alpha_H \left(1 + .201 \; Re^{-1/4} \left[\ell n \, \alpha_P \, \alpha_H - \ell n \, \alpha_P \right] \right)} \right\}$$

33. Compute resistance of perforated plate (gauze) - K_p

$$K_p = 1.21 \, \alpha_p^{-2} - 1$$

34. Compute flow angle ratio of honeycomb - α_H

$$\alpha_H = \frac{\alpha_p \, \alpha_H}{\alpha_p}$$

35. Compute resistance of honeycomb - K_H

$$K_H = - \, .201 \, \text{Re}^{-1/4} \, \ln \, \alpha_H$$

2.4 Conservative Design

36. Compare resistance of perforated plate (gauze) for atmospheric turbulence and steady distortion designs (Items 26 and 33). Choose the larger - K_p

37. Compare flow angle ratio of honeycomb for atmospheric turbulence and steady distortion designs. (Items 27 and 34). Choose smaller - α_H

38. Compute honeycomb length to diameter ratio - $\dfrac{\ell}{d}$

$$\frac{\ell}{d} = - \, \frac{1}{\pi} \, \ln \, \alpha_H$$

39. Determine perforated plate open area ratio from Baines and Peterson plot Figure 4- σ_p

40. Determine the maximum mach number of flow incident on the Inflow Control Structure - M_{ICS}.

41. Plot perforated plate thickness, ℓ_p, against hole diameter d_p, using the transmission loss criterion of less than one dB in the 24th one - third octave band.

$$\ell_p = 5.39 . 10^{-3} \left[5.04 - \left(2 + K_p \, M_{ICS} \right)^2 \right]^{1/2} \sigma_p - \left(1 - \sigma_p \right) d_p$$

42. Select a perforated plate thickness and hole diameter consistent with the estimate of d_{ICS} in Item 10.
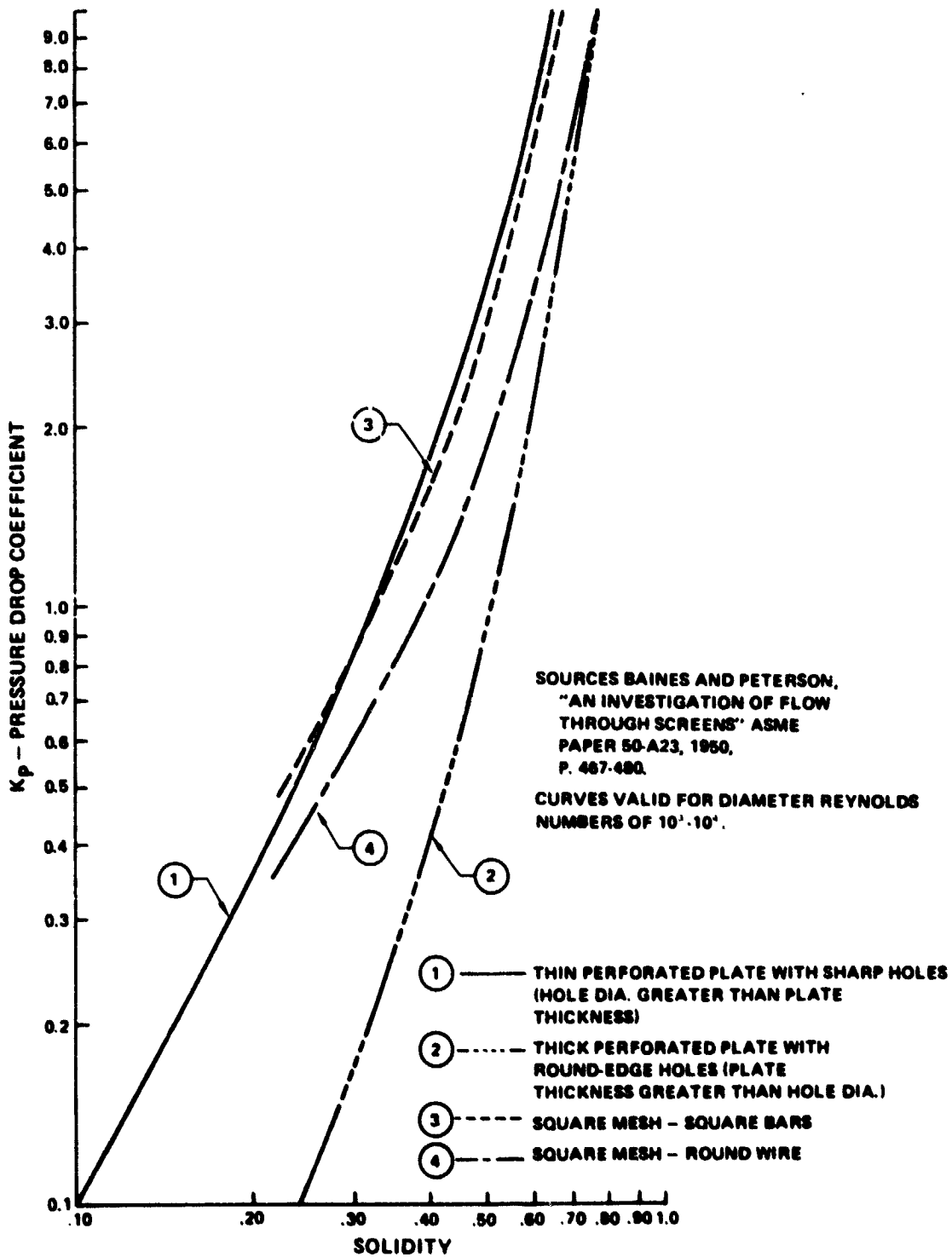
Figure 4   *Pressure Loss Coefficient is a Function of Solidity*

3.0 STATIC TEST PROCEDURES, DATA ACQUISITION/ANALYSIS PROCEDURES

In Section 2 a design system for an Inflow Control Structure has been out-
lined. Such Inflow Control Structures will reduce the differences in fan noise
due to inflow distortion between static and flight conditions. However, numer-
ous other causes for differences in fan noise between the two conditions still
remain. Some of these differences can be minimized by the use of proper static
test procedures and proper data acquisition and analysis, others are not well
understood and need further research. This section provides recommendations
concerning static test procedures and data acquisition/analysis procedures.

3.1 Test Stand Structure

The test stand structure causes distortions in the fan inflow field and af-
fects the sound pressure field generated by the engine. Minimization of these
effects should be considered in future test stand designs.

3.2 Inlet Geometry

The inlet geometry affects the mean flow field as well as the boundary layer
in the inlet. It also impacts the sound pressure field radiating into the for-
ward arc. Based on the information presented in References 7, 8 and 9 and Ap-
pendix II of Reference 3, it is recommended that:

-   The inlet contour between throat and fan face used in static
    tests should match the flight inlet contour.

-   The exterior bellmouth should be minimized in size to a point
    where it still provides small peak velocities in the throat
    highlight area and a well attached boundary layer at the fan
    face. The bellmouth used in the static test configuration of
    Reference 10, satisfies these requirements. Its cross section
    is elliptic and its normalized half diameters are (See Figure
    5A).
    $$\frac{a}{R_0} = .4 \qquad \frac{b}{R_0} = .25$$

48
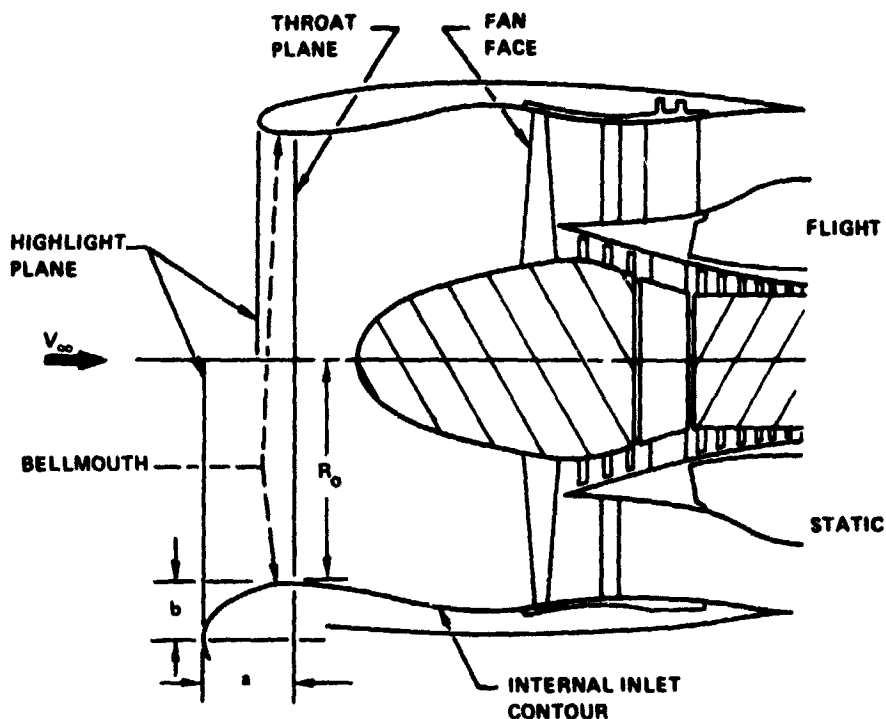
Figure 5   *Inlet Geometry*

3.3 Engine Geometry

The significance of the three dimensional character of the sound pressure
field radiating from a turbofan engine is not known at the present time (see
Appendix II of Reference 3). Until the significance of this phenomena has been
evaluated, it is recommended that the engine geometry be kept identical be-
tween static and flight tests.

3.4 Nozzle Geometry

The use of an Inflow Control Structure results in a negligible pressure drop,
and therefore does not alter the fan operating conditions. However, the fan
operating line differs between static and flight conditions due to the ram
pressure rise in flight. Based on the simple analysis presented in Appendix II
of Reference 3, it is concluded that the operating lines could be matched by
the use of a variable fan exhaust nozzle in static tests. The effect of the

changes in the fan operating line on the fan noise generation are not well known at the present time. Until the magnitude of the resulting differences in the fan sound pressure field have been evaluated, it is recommended that the fan exhaust nozzle hardware be identical for static and flight tests.

3.5 Instrumentation Recommendations

Acoustic Instrumentation

The acoustic instrumentation for static fan noise tests consists of a circular array of microphones at a distance of 20 to 40 inlet diameters from the engine. Based on extensive experience with ground and pole microphones an array of ground microphones and/or pole microphones is recommended. An example showing suggested spacing is shown in Figure 6.

● GROUND MICROPHONES
✕ POLE MICROPHONES
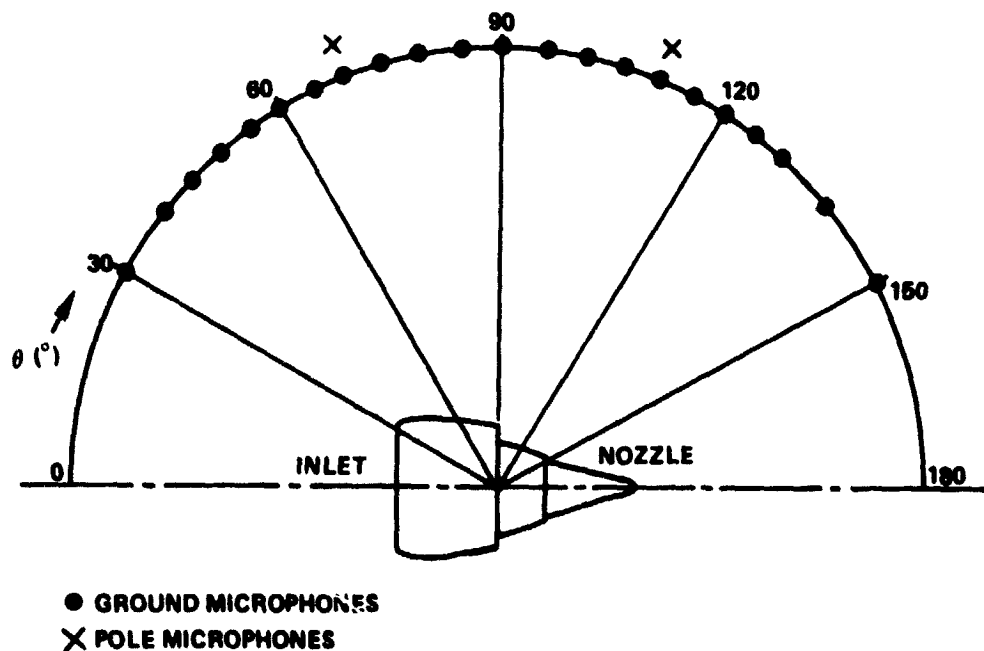
Figure 6   Microphone Array for Static Fan Noise Tests

One-half inch condensor microphones are recommended. They provide essentially
flat frequency response from 40 to 10 KHZ at grazing incidence, are rela-
tively insensitive to temperature and humidity variations, and can be cali-
brated electrostatically.

The ground microphones are mounted 1/2 inch above the ground facing downwards.
The microphone support mounted on a thin flat plate bonded to the concrete
surface must be designed to have negligible effects on the sound pressure
field. Cables should be routed from the far side of the array to the
microphones and should be brought underground if they cross the test arena.

Microphone specifications should be the same as in FAR Part 36 Appendix A.

Meteorological Instrumentation:

Atmospheric conditions within the test arena affect tone noise generation as
well as the sound propagation from the engine to the far-field microphones.
The atmospheric conditions are characterized by the following parameters:

p	(atm)	static pressure
T	^{0}C	static temperature
RH	%	Relative humidity
V_w	m/s	Wind velocity
δ^w	^{0}	Wind direction relative to inlet axis.

In a first order approximation the acoustic pressure is proportional to the
ambient pressure. However, most static tests are conducted close to sea level
altitudes and therefore the ambient pressure covers only a small range. For
practically all static test conditions, corrections for static pressure
changes are not necessary.

Temperature and humidity affect the atmospheric absorption. Ambient temper-
ature is expected to vary only weakly in a horizontal plane, but it can be a
strong function of height above ground. In static tests with ground micro-

51

phones, it is recommended that the ambient temperature be measured at several heights between the ground and the engine height. The following measurement heights are suggested: the microphone heights, at the engine centerline, near the humidity measuring device, and one foot off the measurment surface.

The absolute humidity is not expected to vary significantly within the test arena. The relative humidity will however change with the temperature. Several ambient temperatures (i.e., as specified above) and a single dew point measurement within the test arena are expected to provide sufficient information about the relative humidity distribution. Ambient and dew point temperature measurement accuracy should be .3°C. This will provide an acceptable relative humidity accuracy of $\pm 3\%$.

Wind velocity and direction can affect fan noise sources as well as sound propagation. Wind velocity restrictions in static engine tests are not well defined. A low threshold, air bearing cup anemometer provides wind velocity information of sufficient accuracy ($\pm .22$ M/S between .147 and 6.71 M/S). Since wind velocity and direction may vary significantly over the duration of a test point, they should be recorded continuously for each test point.

Engine Performance Instrumentation:

Instrumentation for all standard engine performance parameters should be available. Engine performance instrumentation to satisfy general and specific measurement needs are required to ensure stable, repeatable, and comparable engine operating characteristics when conducting noise measurement tests. Noise tests conducted on high bypass ratio fan engines require accurate measurement of several important fan parameters. Among these are fan rpm, fan pressure ratio, fan mass flow rate, fan temperature ratio, engine thrust, and fan exhaust area. Additional engine performance parameters are required when measuring particularly for jet exhaust noise generation. These parameters include nozzle temperatures and pressures, overall pressure ratio, and primary engine exhaust area. A total engine noise test would require at least all of the above mentioned parameters plus any other special flow and aerodynamic parameters that might be required for special noise tests. Ambient conditions

52

of temperature, atmospheric pressure, humidity, and wind speed and direction must also be measured as described above, in order that the measured engine performance parameters can be corrected to standard conditions for effective noise measurement comparisons.

3.6 Test Condition Recommendations

In this discussion the term test point is used to describe a time period during which acoustic data are acquired while the engine operates in a stabilized condition.

Test Point Characteristics:

Each test point is characterized by a set of corrected engine parameters (corrected rotational speeds, corrected mass flow rates, component pressure ratios). For typical static test conditions, the relationships between the various corrected engine parameters are unaffected by the ambient atmospheric conditions. A single corrected engine parameter can therefore be selected to characterize the various test points. In static tests concerned with fan noise, it is reasonable to select one of the parameters that describe the thermodynamic cycle of the fan. The corrected fan speed $N1/\sqrt{\theta}$ which is directly related to the fan tip Mach number is one of the corrected parameters that describes the fan cycle. It is easily measured and provides a reliable signal. It is suggested that $N1/\sqrt{\theta}$ be used to characterize the test points in static fan noise tests.

Engine Operating Point Variability for a Test Point:

Engine transients between test points result in very low frequency thermodynamic transients in various engine components. In order to provide stable engine operating conditions at a test point, a stabilization period of at least 2 minutes is recommended before each test point. Unsteady distortions in the inflow field of engines typical for static test conditions cause signifi-

53

cant fluctuations in the engine operating conditions. These fluctuations are greatly reduced with an Inflow Control Structure. Without an Inflow Control Structure corrected speed fluctuations for a test point vary typically 1 percent of the corrected fan speed. With an Inflow Control Structure they are reduced to about .3 percent. Corrected fan speed differences between the various engines on an aircraft in a flyover noise test are typically in the order of 1. percent of the average corrected fan speed. The reduced corrected fan speed fluctuations in static tests with inflow control will likely result in lobular directivity patterns at the fan BPF and its harmonics. It is necessary to consider how to use the static data, with its lobular directivity pattern, to predict flight, which also has lobular directivity patterns and engine to engine speed variations, which tend to average out the lobular patterns.

There are two methods for accounting for this variation. The first method is to obtain static noise data at many fixed corrected speeds, predict flyover noise levels at a series of corrected speed values simulating a typical flyover speed variation, and average the resulting predictions. The second method is to simulate the flyover corrected speed variation during the data acquisition in a static noise test and predict a single flyover noise level from the static measurement.

The two methods differ fundamentally in the procedure for simulating the corrected speed variation in flyover measurements. In the first method the corrected speed variation is directly simulated by making flight noise predictions at a series of corrected speeds while in the second method the flyover speed variation is simulated in the static data acquisition process. The second method is an approximation to the procedurally correct method one and will produce the same answer as method one only if the transformations that are used to predict flight noise levels from static measurements are linear. However, the second method may be more practical to implement than method one.

In addition to being more practical, the second method has two other advantages. First, analysis of the effect of an inlet control screen on fan noise directivity has demonstrated that, for a specific source structure, the screen

54

can, if it contains discontinuities, alter the source directivity via diffraction effects. These diffraction effects can be eliminated (i.e., average to zero) if the engine speed is varied slightly to produce a varying source structure. (It should be noted that the contractors experience with Inflow Control Structures on the JT9D engine has shown these diffraction effects to be small). Second, fan noise directivity is very lobular and sensitive to corrected speed, and varying corrected speed slightly during a static test will produce a better estimate of fan noise at a nominal speed than data obtained with corrected speed held strictly constant. In the past, before the use of an Inflow Control Structure, the fan directivity patterns that were measured were much smoother. Accordingly, problems presented by the lobular directivity patterns were not encountered, and neither of the above methods have been used by Pratt & Whitney Aircraft and Boeing. A variant of the first method has been used where a relatively smaller number of speed points were used to define the noise versus speed characteristics of the engine, and flight predictions were made for a nominal flight speed. Therefore it is difficult at this time to select one of the methods as being the preferred one. The selection is best made by the user depending on constraints unique to his case, e.g. test time, test costs, available data reduction and processing equipment, etc.

Duration of Test Point:

One-third O.B. spectra for the 40 Hz to 10 KHz frequency range are usually based on samples of a duration of 32 seconds. A test point duration of 1 minute is recommended. A minimum of three repeat points per test point is recommended.

Temperature and Relative Humidity Restrictions:

In flyover testing with its inherently long propagation distances between the source and the microphone, atmospheric absorption has a significant effect on the measured data. In this situation a tight restriction on air temperature and humidity is required (FAR PART 36 test window, Figure 7). In static tests the propagation distances are much shorter and a less restrictive test window is acceptable. In the past, static test windows have usually retained the relative humidity limits (20 to 95%) as well as the no precipitation condition.

ATMOSPHERIC ATTENUATION AT 8 kHz (dB/100 M)
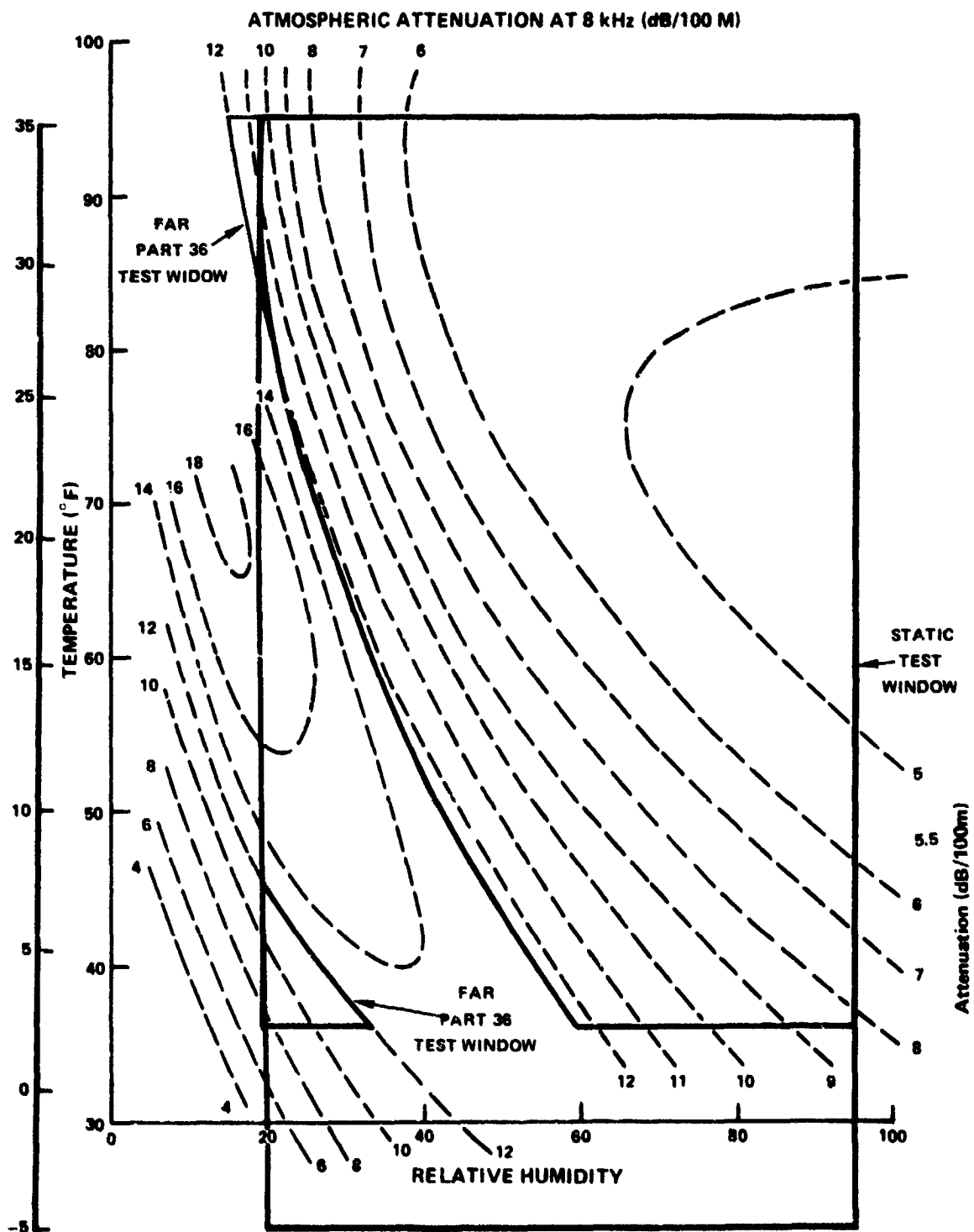
Figure 7   Recommended Test Window

The lower temperature limit has, however, frequently been extended to lower temperatures (25 to 30°F), dependent on the expected environmental conditions. The maximum attenuation limit (12 dB/100 meter at 8 KHz) is frequently waived as well in static tests. A static test window with relative humidities between 20 and 95%, no precipitation and temperatures between -5 and 35°C is recommended for static tests (see Figure 7).

Wind Velocity and Direction Restrictions:

In static tests with an Inflow Control Structure the wind limitations should be based on the following criteria:

- no shadowing of far-field ground microphones
- no reingestion

Observation of the on-line 1/3 OB spectra from the pole and ground microphones at the same angular location provides information about the first limit. If the difference of the spectrum levels in the high frequency range (f > 5 kHz) between the ground microphone and the pole microphone fluctuate or become significantly less than 3 dB, then ground microphone shadowing has occurred and the acoustic data is not acceptable. Extensive testing within the wind envelope shown in Figure 3 has prevented the occurrence of ground microphone shadowing in all tests.

It is recommended that the wind limits presented in Figure 3 be used in static tests.

3.7 Data Acquisition and Processing

Acoustic Data:

The acoustic system should consist of microphone, cathode follower, microphone power supply, preamplifier and recorder. The system should conform to the specifications for noise recording systems as described in FAR Part 36, Appendix A.

57

Data Recording Requirements:

Fourteen (14) channel tape recorders should be used in the FM mode at tape speeds of 30 IPS. Twelve (12) channels should be used for acoustic data, the remaining two (2) channels for voice commentary and the time code. Acoustic data records of 60 seconds duration are recommended.

System Calibrations:

Microphone Calibration:

Before each test series a free-field frequency response calibration should be made for each microphone at the preferred 1/3 O.B. center frequencies between 40 Hz and 10 KHz. The free-field calibration should be accomplished by applying free-field corrections to an electrostatic pressure calibration.

Microphone System Response:

Before the test, electrical signals should be inserted into each microphone system at the microphone preamplifier and measured at the input to the tape recorder amplifiers. The insert signals should be sine waves at the 1/3 octave band (O.B.) center frequencies between 40 Hz and 10 KHz.

Record and Playback System Response Calibration:

Before the test, electrical signals should be inserted simultaneously at all channels of the recorder amplifier inputs. The resulting signals from the playback system determine the record/playback system response. The inserted signals may be sine waves at the 1/3 O.B. center frequencies between 40 Iz and 10 KHz or broadband signals.

1/3 O.B. Analyzer Calibration:

Approximately every two months the filters of the 1/3 octave band (O.B.) analyzer should be calibrated for bandwidth and level.

58

Microphone System Sensitivity Calibration:

A microphone system sensitivity calibration should be made every test day before the first test point and after the last test point. The system sensitivity should be checked for each microphone system using a piston phone operated at 250 Hz.

Magnetic Tape Calibration:

At the beginning of each magnetic tape reel a 124 dB equivalent sine wave reference signal at 250 Hz should be applied to all channels simultaneously for a period of 30 seconds.

Data Reduction:

The acoustic data are analyzed with a 1/3 O.B. analyzer. The following corrections are applied in order to produce free-field 1/3 O.B. spectra:

- Microphone pressure response based on the electrostatic calibration of each microphone.

- Microphone pressure to free-field response. Provided by the microphone manufacturer for each microphone type.

- Microphone system response based on the results from insertion calibration conducted before the test.

- Microphone system sensitivity based on the daily calibration with piston phone.

- Record to playback response based on the results of the calibration conducted before the test.

- Magnetic tape sensitivity based on the calibration signal recorded in the initial segment of each tape.

- 1/3 OB analyzer filter level and bandwidth correction based on the bi-monthly calibration of the analyzer.

- Atmospheric absorption. Correction to FAA standard day $T = 25^{\circ}C$ ($77^{\circ}F$), relative humidity 70% based on Reference 12.

- Pressure doubling in ground microphones. All 1/3 OB levels are reduced by 6 dB in order to correct to free-field conditions.

Data are analyzed for all microphones at all test points.

4.0 PROJECTION OF STATIC DATA TO FLIGHT

In Section 3.0, techniques for obtaining appropriate engine data during static testing with an Inflow Control Structure were described. As a result of these techniques, free field spectra for each microphone angle and test condition (i.e. corrected speed) were obtained, corrected to FAA day temperature and humidity ($77^{\circ}F$, 70% RH). The use of these data to predict engine noise spectra as a function of position during an aircraft flyover is described in this section.

4.1 Specification of Aircraft Configuration, Flight Path and Atmosphere

1. The first step is to define the engine/nacelle flight path and engine operating condition during the flyover. Constant airplane velocity, rate of climb, and engine operation will be assumed during the flyover. The flight path is defined by the trajectory of an engine reference point and is specified by its slope and altitude above the ground reference point, as defined in Figure 8. The orientation of the engine relative to the flight path must also be known.

2. The temperature and humidity will be assumed to be uniform with altitude and equal to those for an FAA day, ($77^{\circ}F$, 70% RH) since noise certification data must be corrected to these conditions.

60

4.2 Calculation of Acoustic Emission Angle Versus Flyover Time

3. The sideline location of the microphone for which the flyover prediction is to be made is specified by the distance x, (see Figure 8).
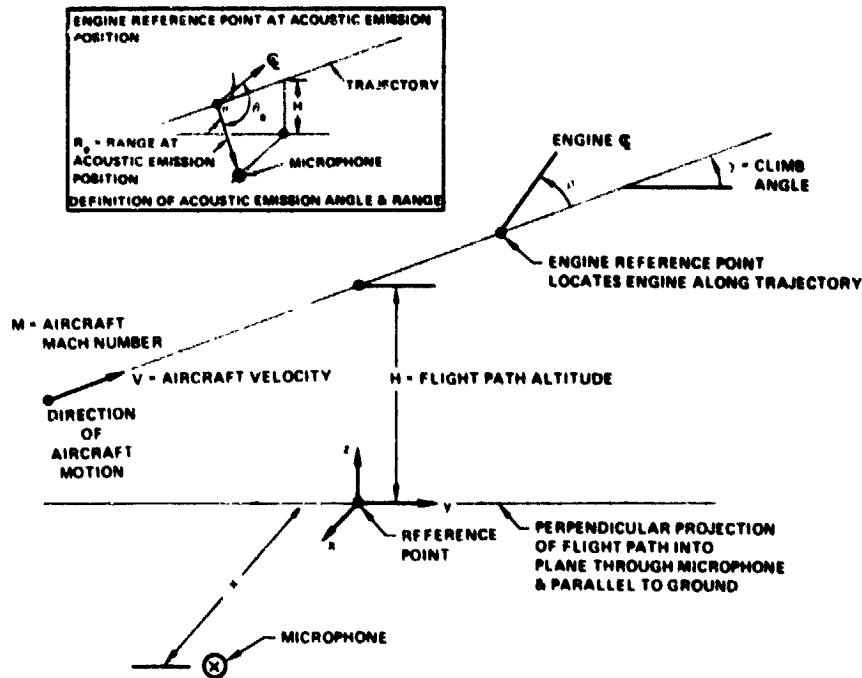
Figure 8   Definition of Flight Path Parameters

4. Zero time is equal to the time when the engine reference point is directly over the ground reference point. Using this definition, and knowing the flight path altitude above this reference point and the aircraft's velocity and rate of climb, the acoustic emission angle can be calculated as a function of time from:

$$\theta_e = 180 - \cos^{-1}\left[\frac{(Vt - MR_e)\cos\beta + M\sin(\gamma + \beta)}{R_e}\right] \qquad (1)$$

where R_e is the acoustic range, or distance from the source to the microphone, given by Equation (2).

$$R_e = \frac{\sqrt{(Vt)^2 + 2VtH \sin\gamma + H^2 (1-M^2\cos^2\gamma) + X^2 (1-M^2)} - M[Vt+H\sin\gamma]}{(1-M^2)} \quad (2)$$

(symbols for Equation (1) and Equation (2) are defined in Figure 8).

5. The time duration for the calculation is next selected. (Note that for certification predictions, the time duration is selected to ensure a 10 PNdB range in noise level.)

6. Break the time duration into desired intervals (for certification predictions, one half second intervals are usually selected) and calculate the corresponding emission angles Θ_e, and acoustic ranges, R_e from Equation (1) and Equation (2).

4.3 Preparation of the Static Data for Projection to Flight

7. Engine spectra must be defined for the engine operating condition specified in Step 1. Since data are not usually available at the precise operating condition specified, interpolation of the data as a function of operating condition is required. For this, and subsequent processing of the data, it is necessary to isolate the various contributing components to the total spectra, i.e., jet, combustion, turbine, fan. There are no set procedures for accomplishing this breakout, although component spectra are usually obtained by using prediction systems for at least some of the components as guides. (If flight projections of the fan tone are desired, then it is a simple matter to identify these tones from the spectra.) Once the contributing sources have been isolated, interpolation as a function of the appropriate performance parameter is carried out (e.g. corrected speed for fan noise, primary jet velocity for jet noise). For

fan noise, it is recommended that interpolation procedures be used
that curve fit all the data to minimize the difference between the
data and the values given by the curve fit. In this manner, local
anomalies in the variation of noise with speed are minimized.

Corrections for the effects of the Inflow Control Structure on the
radiated sound field should be applied. Based on results presented in
Reference 6, these effects are small compared to the variability in
measured data and the corrections will be taken to be zero.

8. At this point, recognition has to be taken of the fact that static
    data is acquired at fixed (even) angles relative to the engine cen-
    terline, while flight test data is averaged over flyover time inter-
    vals (.5 seconds is a typical integration time) which cover a finite
    angular range. To achieve agreement between the measured static data
    projected to flight, and the flyover data presented in even time in-
    tervals it is necessary to simulate the averaging process that takes
    place in flight. In a simple approximation of the actual process the
    spectra from all angles that fall within a time interval are loga-
    rithmically averaged to represent the time average for the flyover
    condition. If none of the measurement angles fall within the one-
    half second interval (unlikely to occur except for values of Θ_e
    close to 0 and 180 degrees, if microphone angle spacing used during
    the static test program is 10 degrees or less), then interpolation is
    required for that interval.

9. For each emission angle defined in Step 6, project, for an FAA day,
    the spectra from the measurement distance used in the static test to
    the distance specified by the acoustic range. This is accomplished in
    two parts, first by accounting for spherical attenuation, Equation
    (3), and then by accounting for air attenuation effects using
    Reference 11.

$$\Delta SPL \text{ (dB)} \atop \text{spherical} \atop \text{attenuation} \quad = 20 \log \frac{R \text{ static measurement}}{R_e} \qquad (3)$$

63

This step provides static free field spectra for each emission angle, projected to distances consistent with the flyover path defined in Step 1.

4.4 Inclusion of Aircraft Installation Effects

10. Effects of wing shielding and reflection, fuselage shielding and jet flow shielding on each component of engine noise may now be included. Modules describing these effects are currently under development as part of the NASA ANOPP procedure. In the absence of these modules, it is recommended that simple analytical models be developed.

4.5 Projection of Static Free Field Spectra to Flight Free Field Spectra

11. Source reduction and convective amplification effects due to flight are corrected for at this point. The jet component is corrected to account for source reduction due to the motion of the jet through the air and for convective effects. Reference 12 is recommended for such corrections.

    The remaining components, fan, turbine, and combustion noise are modified for the effects of convective amplification by addition of Equation (4).

$$\Delta SPL \text{ (dB)}_{\substack{\text{Convective} \\ \text{amplification}}} = -40 \log \left[1 - M \cos \theta' \right] \tag{4}$$

12. The sources, except for jet, are then shifted in frequency to account for Doppler effects, as defined in Equation (5). The resultant spectra are then summed.

64

$$\frac{f}{f_0} = \frac{1}{1 - M \cos \theta'}$$ (5)

Where f = frequency at flight condition

f_0 = frequency at static condition

(Note that only the frequencies are shifted in this step, the spectral amplitudes remain unchanged.) If one third octave band analysis has been used to define the spectra, then, after doppler correction, the energy should be redistributed into the standard one-third octave bands.

At this point, free field flyover spectral estimates have been generated from the static data for the engine/nacelle combination tested, the defined flight path, and the specified installation effects.

4.6 Inclusion of Ground Effects

13. The presence of the ground surface results in extra attenuation, not accounted for in any of the above corrections, and this is particularly important for microphones located away from the flight path. Reference 13 can be used for this correction.

14. Effects of ground plane reflections can be accounted for by use of methods such as those described in Reference 14. Ground impedance is required as an input, but very little data is available on values of ground impedance encountered during aircraft flyovers. References 15, 16, and 17 are sources of this information, for grass and sandy surfaces.

4.7 Inclusion of Multiple Engine Effects

15. The effect of multiple engines is next included by:

65

a)   If engine separation is large, repeating the above steps for each of the remaining engines and then summing the resulting spectra (by use of anti-logarithmic addition), after displacing the engine time scales by the amount required to account for their separation distances.

b)   If engine separation is negligible, by adding $10 \log N_e$ to each of the spectra generated in the above steps, where N_e is the number of engines.

At this point, flyover spectral estimates have been generated from the static data for multiple engines that include ground and shielding effects. The spectral time history developed as a result of the above procedures can be used to generate Perceived Noise Level (PNL) flyover histories and Effective Perceived Noise Level (EPNL), the units used in certification procedures defined by FAA FAR Part 36.

The corrections described above for projecting static data to flight are drawn from existing models and information. Some of the corrections have greater sources of error in them than others, and some effects are not accounted for since they are currently not well enough understood. The following discusses major potential error sources in these corrections.

1. Long distance propagation effects in the atmosphere.

a)   Sound is scattered by atmospheric turbulence, an effect which is not included.

b)   Extra ground attenuation, which is included, is presently an empirical correction whose physical origin has yet to be defined.

c)   Non-linear sound propagation effects may become significant at large propagation distances, an effect which is not included.

66

d) Refraction of sound by velocity and temperature gradients is not
    included, although these effects can in part be included by use
    of layered weather atmospheric models.

2. Convective Amplification

a) The convective amplification factor applied to fan and core
    noise has been developed from theoretical models that do not
    fully simlulate the properties of gas turbine engine noise
    sources, and the application of this factor has not been veri-
    fied experimentally.

5.0 LIST OF SYMBOLS & ABBREVIATIONS

Symbol	Unit	Description
a/R_o, b/R_o	-	Normalized Half Diameters of Bellmouth Inlet Ellipse
dB	-	Decibel
d_{ICS}	M	Maximum Characteristic Dimension of Inflow Control Structure Material (e.g. honeycomb cell size)
f	Hz	Frequency
f_o	Hz	Doppler Shifted Frequency
H	M	Flight Path Altitude
ICS	-	Inflow Control Structure
k_1^*	M^{-1}	Wavenumber, defined in Step 19 of Section 2.0
k_{2L}	M^{-1}	Wavenumber, defined in Step 19 of Section 2.0
k_{2U}	M^{-1}	Wavenumber, defined in Step 19 of Section 2.0
k_{3L}	M^{-1}	Wavenumber, defined in Step 19 of Section 2.0
k_{3U}	M^{-1}	Wavenumber, defined in Step 19 of Section 2.0
K_H	-	Honeycomb Resistance
K_p	-	Perforated Plate Resistance
L_{AF}	M	Characteristic Length Scale of Turbulence In Flight Case
L_{AS}	M	Characteristic Length Scale of Turbulence In Static Case
L_{ICS}	M	Characteristic Length Scale of Turbulence Behind Inflow Control Structure
ℓ_{1F}	-	Final Contraction Ratio (Inflow Control Structure to Fan Face)
ℓ_{1S}	-	Static Contraction Ratio

68

Symbol	Unit	Description
ℓ/d	-	Honeycomb Length to Diameter Ratio
ℓ_p	M	Perforated Plate Thickness
M	-	Aircraft Mach Number
M_{ICS}	-	Maximum Mach Number Incident to Inflow Control Structure
N	-	Rotor Blade Number
$N_1/\sqrt{\theta}$	Rev/S	Corrected Fan Rotor Rotational Speed
N_e	-	Number of Engines
N_F	M/S^2	Turbulence Field Characteristic, Defined in Step 20 of Section 2.0
Re	-	Reynolds Number of Honeycomb Cell
R_e	M	Acoustic Range (See Figure 8)
R_{ICS}	M	Nominal Radius of Inflow Control Structure
R_o	M	Inlet Radius at Fan Face
t	S	Time
ΔU_{1A}	M/S	Streamwise Velocity Deficit in Wake Before Contraction
U_{2A}	M/S	Maximum Azimuthal Velocity in Vortex Before Contraction
U_A	M/S	Maximum Wind Velocity In Test Window
$\sqrt{U_{AF}{}^2}$	M/S	Root Mean Square Value of Turbulent Velocity In Flight
$\sqrt{U_{AS}{}^2}$	M/S	Root Mean Square Value of Turbulent Velocity Statically
U_{ICS}	M/S	Throughflow Design Speed at Inflow Control Structure
U_{REF}	M/S	Static Reference Wind Speed
U_o	M/S	Inlet Velocity at Lowest Speed of Interest Along Engine Operating Line
V	M/S	Aircraft Velocity

Symbol	Unit	Description
X	M	Sideline Location of Microphone
Z	M	Engine Centerline Height Above Ground During Static Test
Z_0	M	Roughness Scale
Z_{REF}	M	Reference Height
α_H	-	Flow Angle Ratio - Honeycomb
α_p	-	Flow Angle Ratio - Perforated Plate
β	degrees	Angle Between Nacelle Centerline and Flight Path
γ	degrees	Climb Angle
γ_F	M^{-1}	Turbulence Field Characteristics Defined in Step 20 of Section 2.0
γ'	degrees	Blade Relative Inflow Angle
λ_{min}	M	Minimum Sensitive Transverse Scale
$(\lambda_{min})_{ICS}$	M	Minimum Sensitive Transverse Scale at Inflow Control Structure
Θ	-	Ambient Static Temp(^{0}K)/288^{0}K.
θ_e	degrees	Angle Between Nacelle Centerline and Vector from Acoustic Emission Position to Microphone (See Figure 8)
Θ'	degrees	Angle Between Flight Path and Microphone Measured from Acoustic Emission ╌:ition (See Figure 8)
ν	M^2/S	Kinematic Viscosity of Air
σ_p	-	Open Area Ratio For Perforated Plate

70

6.0 REFERENCES

1. Atvars, Y. and Rogers, D. F. "The Development of Inflow Control Devices for Improved Simulation of Flight Noise Levels During Static Testing of a HBPR Turbofan Engine", AIAA paper 80-1024, June, 1980.

2. Rogers, D. F. and Ganz, U. W. "Aerodynamic Assessment of Methods to Simulate Flight Inflow Characteristics During Static Engine Testing", AIAA paper 80-1023, June 1980.

3. Peracchio, A., Gedge, M., Ganz, U.W. and Robbins, K "Forward Speed Effects on Fan Noise - Procedures for Static Testing", Contractor Final Report - NASA Contract NAS1-15085, NASA CR 165626, Sept 1980.

4. Ganz, U. W. "Analytical Investigation of Fan Tone Noise Due to Ingested Atmospheric Turbulence", Phase I Final Report, NASA Contract No. NAS1-15085, NASA CR 3302, August 1980.

5. Gedge, M. R. "Analytical Models for Use in Fan Inflow Control Structure Design", Phase II Interim Report, NASA Contract No. NAS1-15085, NASA CR 159189, 1980.

6. Gedge, M. R., A Design Procedure for Fan Inflow Control Structures", Phase II Final Report, NASA Contract No. NAS1-15085, NASA CR 165625, Sept 1980.

7. Ganz, U. W. "Parametric Study of the Fan Inflow Field in Static and Flight Tests", Boeing Document D6 - 49669, May 1980.

8. Mathews, D. C. and Nagel, R. T., "Inlet Geometry and Axial Mach Number Effects on Fan Noise Propagation", AIAA Paper 73-1022, October 1973.

9. Clark, T. L., "Investigation of the Effects of Inlet Shape on Fan Noise Radiation", Final Report, NASA Contract NAS1-15394, January 1981.

10. Aerospace Recommended Practice, ARP 866, August 1964.

11. Anon, "SAE Aerospace Recommended Practice" ARP 866A, March 15, 1975.

12. Stone, J. R. "An Improved Method for Predicting the Effects of Flight on Jet Mixing Noise" NASA TM 79155, 1979.

13. Dunn, D. G. and Pearl, N. A. "Aircraft Noise Source and Contour Estimation", NASA CR 114649 (Section 5.1.3.1), July 1973.

14. Yoerkie, C. A. and Larson, R. S. "Prediction of Free-Field Noise Levels from Pole Microphone Measurements", AIAA Paper No. 80-1058, June, 1980.

15. Embleton, T. F. W., Piercy, J. E.; and Olson, N. "Outdoor Sound Propagation Over Ground of Finite Impedance", J. Acoust. Soc. Am., Vol. 59, No. 2, February, 1976.

16. SAE Committee A-21 "Acoustic Effects Produced by a Reflecting Plane" SAE AIR 1327, January 15, 1976.

17. Dickinson, P. J., and Doak, P. E. "Measurements of the Normal Acoustic Impedance of Ground Surfaces", J. Sound and Vib., Vol. 13, No. 3, November, 1970.

18. Engineering Sciences Data Unit, "Characteristics of Atmospheric Turbulence near the Ground (Part III)," ESDU Item, Number 75001, July, 1975.

Discussion of Test Procedures

1.0 Introduction

Test procedures for static testing are discussed in this appendix. The proce-
dures defined in the Procedures Report were selected based on these discus-
sions. The following considers the test stand configuration, inlet and fan
nozzle geometry effects, and engine sound field effects. Instrumentation re-
quirements, both acoustic and meteorological and test condition considerations
are then discussed.

2.0 Test Stand, Inlet, Engine and Nozzle Geometry

2.1 Test Stand

The static test stand structure may affect the fan inflow field as well as the
noise radiation from the engine. Data from the fan rotor blade mounted trans-
ducers acquired during the Pratt & Whitney Aircraft/Boeing Joint Noise Program
demonstrated the significance of stand structure related distortions in the
fan inflow field. The blade mounted transducer data also showed that outside
of the inlet boundary layer the usage of an Inflow Control Structure (ICS)
reduced these distortions. Although the Inflow Control Structure reduces test
stand structure related inflow distortions, it is recommended that future
designs of test stand structures consider the minimization of fan inflow
distortions.

2.2 Inlet Geometry

The inlet geometry affects the fan inflow field as well as the sound propaga-
tion from the fan into the forward arc. Flight inlets are composed of a small
bellmouth and a diffuser (Figure 1). They are designed to provide good inlet
recovery in all flight conditions. In static operation however the flight in-
let produces high velocity peaks between the highlight and the throat planes.
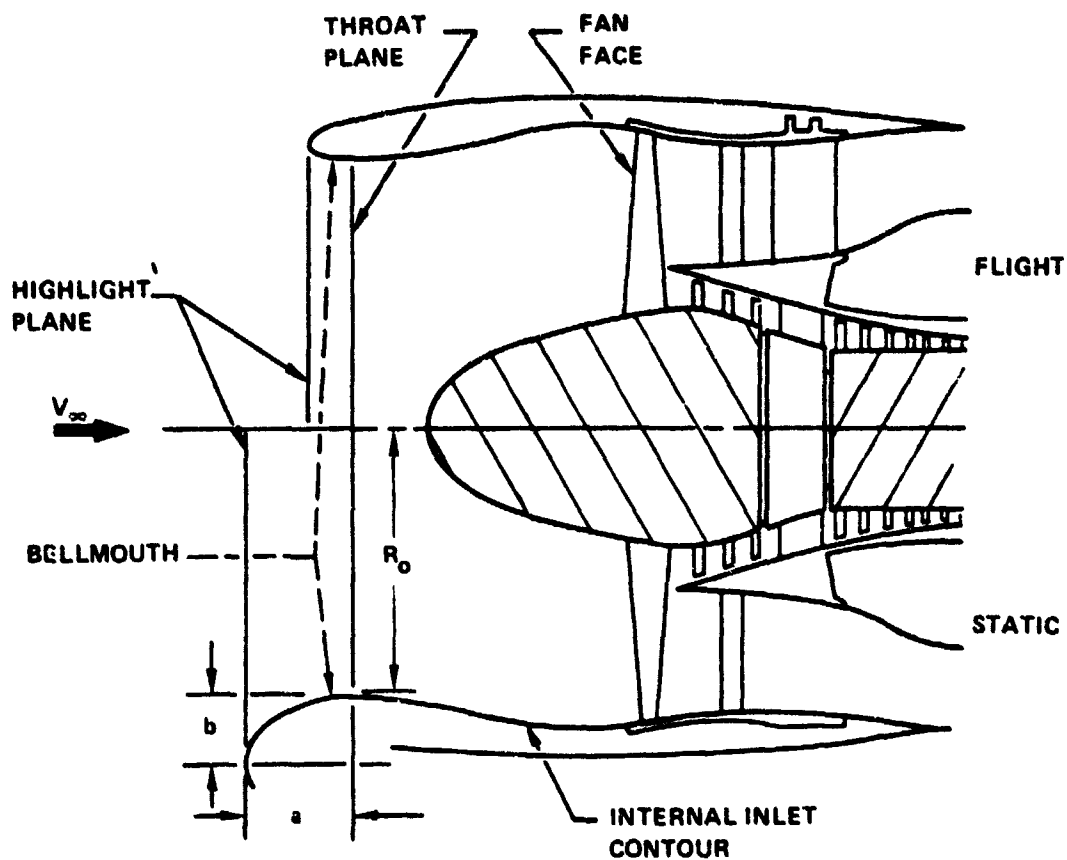
73

Figure 1   Inlet Geometry

These velocity peaks are caused by the large variation in the streamline cur-
vature in the flow field, the pressure gradients necessary to sustain it and
the resulting pressure minima at the bellmouth surface. The diffusion from
these velocity peaks to the fan face also result in a thicker boundary layer
and a boundary layer condition closer to separation in static tests. These
deficiencies in the static inflow field can be improved to some extent with a
larger bellmouth attached to the flight inlet diffuser. The mean flow velocity
field between the throat and the fan face are nearly the same for static and
flight conditions if a large bellmouth is used in the static situation. The
boundary layer thickness at the fan face will however always be thicker in
static conditions, independent of the bellmouth size. Analytical studies have
indicated that the boundary layer thickness has a shallow minimum for an in-
termediate size bellmouth (Reference 1). For a small bellmouth the excessive
boundary layer thickness is due to the increased diffusion necessary between

74

the peak velocities and the fan face. For very large bellmouths the excessive thickness is due to the large length over which the boundary layer develops. Independent of bellmouth size, the inlet boundary layer in static tests is expected to be larger than the one in flight. Simulation of a flight inlet boundary layer in static tests can be achieved by:

- modification of the internal inlet contour between the throat and the fan face

- boundary layer treatment (suction or blowing)

The inlet geometry also affects the sound propagation and radiation into the forward arc. Data presented in Reference 2 demonstrate the significance of the internal contour between the fan face and the throat on the propagation in the inlet. Data presented in Reference 3 show the significance of the external contour on the radiation in the zero flow condition. It is also expected that the mean flow velocity distribution between the throat and the highlight has some effect on the radiation from the inlet.

Based on these observations it becomes clear that a complete simulation of the flight inflow field, the sound propagation in the inlet and the radiation into the forward arc in static conditions is extremely difficult to achieve. A compromise solution is needed that provides the closest simulation of flight conditions in static tests. The information necessary to define such a compromise configuration is incomplete at the present time. However, based on the information presented in References 1, 2 and 3 the following is recommended.

- The inlet contour between throat and fan face used in static tests should match the flight inlet contour.

- The exterior bellmouth should be minimized in size to a point where it still provides small peak velocities in the throat highlight area and a well attached boundary layer at the fan face. The bellmouth used in the static test configuration of Reference 4 satisfies these requirements. Its cross section is elliptic and its normalized half diameters are

75

$$\frac{a}{R_0} = \sim 0.4; \quad \frac{b}{R_0} = \sim 0.25$$

It must however be emphasized that only further research efforts can provide additional insight in this area. Such efforts should include the evaluation of:

- The effect of inlet boundary layer on fan noise.

- The effect of inlet boundary layer on sound propagation.

- The effect of inlet geometry with and without flow on sound propagation and radiation.

- The effect of inlet droop on sound generation, propagation and radiation.

2.3 Engine Geometry

It is usually assumed that fan sound pressure fields are two-dimensional. Based on theoretical considerations, sound pressure fields that are contained within the duct modes of a single spinning order produce two-dimensional sound pressure fields. But in general the farfield sound pressures may be a function of both the cone angle and the polar angle. This is especially true for the deterministic noise sources within the fan stage. The periodicity in the polar angular coordinate is usually related to the differences in the spinning order of the dominating modes; i.e.,

$$\Delta O = \frac{2\pi}{\Delta m}$$

With

$\Delta O =$ period of polar angular

$\Delta m =$ difference in spinning order between dominating modes

If the polar angular variation in the sound pressure field is significant, then measurements in a single polar angular plane may not suffice to define the complete sound pressure field. Polar angular variations may occur particularly in the following sound pressure fields:

- Fan rotor noise at the blade passing frequency and its harmonics due to inflow distortions of low fundamental order (potential field due to pylon or struts in the fan duct, inlet droop related inflow distortions, viscous wakes due to rake mounted inlet sensors).

- Stator noise at higher harmonics (> 3) of the blade passing frequency due to rotor related flow distortions.

Since these observations are based on theoretical considerations, and since experimental evidence is not available, it is recommended that the polar angular dependence of the sound pressure field be evaluated in a future study. Until then, current test techniques, such as those used in obtaining the data of Section 4.4 of the main body of the report should be used.

2.4 Fan Nozzle Geometry

Pressure drops connected with inflow control structures designed using the recommended procedures are low because low values of pressure drop coefficient and velocity through the screen result. Therefore, the use of an Inflow Control Structure has a negligible effect on the fan operating line, so compensation by modifying the fan duct control area is not required. Since the Inflow Control Structure is used to simulate in flight fan operation, the effects of free stream ram pressure rise on the fan operating line must also be considered. Because of the ram pressure rise the fan operating condition at a given corrected speed changes between static and flight conditions. Although the airplane forward velocities are small during the flight conditions of interest, the ram effect at low engine power settings may alter the fan operating point. This subject is explored theoretically in what follows.

77

The mass flow rate through the fan nozzle is computed based on the isentropic flow equations

$$\dot{m} = \frac{P_t}{\sqrt{T_t}} \, A \sqrt{\frac{2}{R} \left(\frac{P}{P_t}\right)^{1/\gamma}} \; \sqrt{\frac{\gamma}{\gamma -1} \left[1 - \left(\frac{P}{P_t}\right)^{\gamma -1/\gamma} \right]}$$

The corrected mass flow rate is therefore only a function of the nozzle pressure ratio (P_t/p) and the effective nozzle area A.

If the fan operating conditions are matched in static and in flight conditions, then the fan nozzle pressure ratio in static conditions is lower by the flight ram pressure.

$$\left(\frac{P_t}{P}\right)_{static} = \left(\frac{P_t}{P}\right)_{flight} \left(\frac{P}{Pt}\right)_{\Delta P}$$

with

$$\left(\frac{P_t}{P}\right)_{\Delta P} = \text{total to static pressure ratio due to aircraft speed.}$$

In order to match the corrected mass flow rates the fan nozzle area must be increased in static test conditions.

For small variations around a given nozzle operating condition, the equation for the corrected mass flow can be approximated by the linear terms of the Taylor series expansion.

78

$$\Delta \frac{\dot{m}\sqrt{T_t}}{P_t} = \frac{\delta\left(\frac{\dot{m}\sqrt{T_t}}{P_t}\right)}{\delta A} \ \Delta A \ + \ \frac{\delta\left(\frac{\dot{m}\sqrt{T_t}}{P_t}\right)}{\delta\left(\frac{P}{P_t}\right)} \ \Delta\left(\frac{P}{P_t}\right)$$

Based on the condition of no corrected mass flow change between static and flight conditions the nozzle area increments for static tests can be computed with the above equation.

$$\frac{\Delta A}{A} \ = \ - \ \frac{1}{\frac{\dot{m}\sqrt{T_t}}{P_t}} \ \cdot \ \frac{\delta\left(\frac{\dot{m}\sqrt{T_t}}{P_t}\right)}{\delta\left(\frac{P}{P_t}\right)} \ \Delta\left(\frac{P}{P_t}\right)$$

The normalized partial in this equation is

$$\frac{1}{\frac{\dot{m}\sqrt{T_t}}{P_t}} \ \ \frac{\delta\left(\frac{\dot{m}\sqrt{T_t}}{P_t}\right)}{\delta\left(\frac{P}{P_t}\right)} = \ \frac{1}{\gamma}\left(\frac{P}{P_t}\right)^{-1} - \ \frac{\gamma-1}{2\gamma}\left(\frac{P}{P_t}\right)^{-1/\gamma}\left[1-\left(\frac{P}{P_t}\right)^{\gamma-1/\gamma}\right]^{-1}$$

The nozzle pressure ratio difference between static and flight conditions for matched fan operating conditions is

$$\Delta\left(\frac{P}{P_t}\right) = \ \left(\frac{P}{P_t}\right)_{static} - \ \left(\frac{P}{P_t}\right)_{flight}$$

$$= \left(\frac{P_{t2.7}}{P_{t2.5}} \ \frac{P_{t2.5}}{P_{t2}} \ \frac{P_{t2}}{P_{t1}} \ \frac{P_{t1}}{P_{am}}\right)^{-1}_{static} - \left(\frac{P_{t2.7}}{P_{t2.5}} \ \frac{P_{t2.5}}{P_{t2}} \ \frac{P_{t2}}{P_{t1}} \ \frac{P_{t1}}{P_{am}}\right)^{-1}_{flight}$$

with

$$P_{t2.7}/P_{t2.5} = \text{fan duct total pressure ratio} = 1.$$

$$P_{t2.5}/P_{t2} = \text{fan pressure ratio.}$$

$$P_{t2}/P_{t1} = \text{inlet total pressure ratio} = 1.$$

$$P_{t1}/P_{am} = \text{total to ambient pressure ratio.}$$

$$= 1. \text{ in static conditions.}$$

therefore
$$\Delta\left(\frac{P}{P_t}\right) = \left(\frac{P}{P_t}\right)_{flight} \left[\left(\frac{P_{t1}}{P_{am}}\right)_{flight} - 1\right]$$

The nozzle increment required in static tests in order to match the flight fan operating condition then becomes

$$\frac{\Delta A}{A} = \left[\left(\frac{P_{t1}}{P_{am}}\right)_{flight} - 1\right] \left\{\frac{\gamma-1}{2\gamma} \left[\left(\frac{P}{P_t}\right)^{-(\gamma-1)/\gamma} - 1\right] - \frac{1}{\gamma}\right\}$$

$$= \left[\left(1 + \frac{\gamma-1}{2}M_\infty^2\right)^{\gamma/\gamma-1} - 1\right] \left\{\frac{\gamma-1}{2\gamma} \left[\left(\frac{P}{P_t}\right)^{-(\gamma-1)/\gamma} - 1\right] - \frac{1}{\gamma}\right\}$$

The above equation indicates that the nozzle area increment increases with the aircraft Mach number to be simulated in the static test. The increment is also a function of the fan nozzle pressure ratio. It becomes large for small pressure ratios and decreases to zero at the critical nozzle pressure ratio.

Results based on the above equation are presented in Figure 2. Since the presented data are based on a linearized equation, they are only valid for small M_ch numbers. The results indicate that for typical aircraft approach conditions the fan nozzle area increments are in the order of 3 to 9 percent. At takeoff conditions the increment becomes very small due to the large fan nozzle pressure ratio. Based on this analysis, in order to match the flight fan operating conditions in static tests at all power settings, a variable fan nozzle geometry would be required. Such a variable geometry will have some effects on the fan noise propagation and radiation into the aft arc, and may also alter the jet noise.
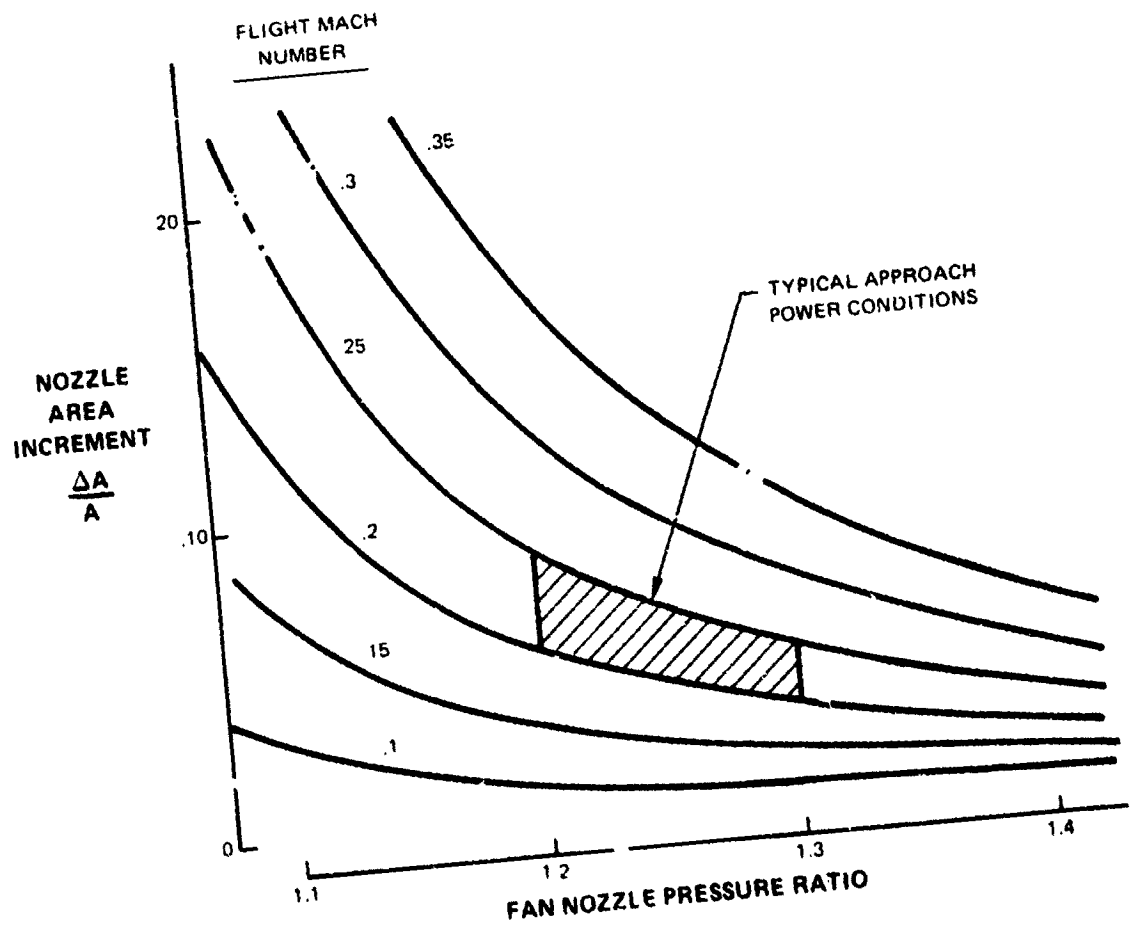

Figure 2   Approximate Nozzle Area Increment Required in Static Tests to Match Flight Fan Operating Condition

Estimates of the effect of fan nozzle area change on radiated BPF noise were obtained from Figure 39 of "Fan-Compressor Noise: Prediction, Research and Reduction Studies" by E. A. Burdsall and R. H. Urban, FAA-RD-71-73, Final Report, February, 1971. This figure shows that tone generated power increases approximately as $10 \log \Delta P$ where ΔP is the fan pressure rise. Using this expression, the effect of the load line variations discussed above on radiated BPF tone is found to be 0.4 dB or less. The test data used to generate these results were obtained from a HBPR fan tested without an inflow control structure, and as such may be misleading. These results are inconclusive, and it is hard at this point to quantify the effect of nozzle area changes on fan radiated noise, or whether the nozzle area should be varied, since it will affect other sources, such as the jet.

Based on these observations, it is recommended that the importance of accounting for the differences in fan operating conditions between static and flight conditions on noise generation be evaluated in future test programs. Until then, current static test techniques using flight nozzle areas, (which as shown in Section 4.4 of the main body of the report, give reasonable agreement between flight projected static data and flight data), should be used.

3.0 Instrumentation

3.1 Acoustic Instrumentation

The acoustic instrumentation in static fan noise tests consists typically of a set of microphones located in the acoustic far-field of the engine. Usually the microphones are arranged in a circular array at a distance of 20 to 40 fan diameters (50 m, 150 ft) from the engine. At the present three different microphone arrangements are used:

- pole microphones
- ground microphones
- combination of pole and ground microphones

82

Pole microphones are normally located at engine axis height above the ground.
Measurements with these microphones are affected by the interference between
the direct and ground reflected signals. The phase relationship between these
two signals is not only a function of geometry and frequency, but also is
affected by the atmospheric conditions within the test arena. Temporal fluctu-
ations in the phase between the two signals cause extreme fluctuations in the
fan tone noise signals received at the microphones. Reasonably certain extra-
polation of measured one third octave band spectra to free-field spectra is
only possible at high frequencies where these effects are minimized.

Ground microphones are placed very close to the ground and provide conditions
close to constructive interference between the direct and indirect signals
throughout the frequency range of interest. Fan tone noise signal strength
fluctuations are significantly reduced relative to the pole microphone sig-
nals. Free-field extrapolation is achieved by a 6 dB reduction of the measured
signals. Refraction of high frequency signals at ground microphones may occur
in excessive temperature or velocity gradients in the test arena. However,
reasonable restrictions on the test weather window will preclude such pro-
blems. In addition, for 1/2 inch microphones, grazing incidence corrections
should be applied to the pressure response of the microphone.

In the combination of pole and ground microphones the signals from the two
microphones are combined. The low freqeuncy signal of the ground microphone is
combined with the high frequency portion of the pole microphone. This approach
eliminates the low frequency problem in the pole microphones and precludes the
potential high frequency problems of the ground microphones. The main disad-
vantages of this approach are the doubling in the number of microphones and
the uncertainties in the merger region between the two spectra.

Aircraft flyover noise data are usually based on averages for samples of 500
milliseconds duration. Angular variations in fan tone noise are fully taken
into account but averaged over large angular segments, especially at the air-
craft overhead position. At this position in the FAR Part 36 approach condi-
tion the data is averaged over about 20 degrees, in the takeoff condition the
corresponding data represents an average over an angle of 10 degrees. Ensemble

averaged data of aircraft flyover noise based on an array of microphones rather than on a single microphone significantly improves angular resolution (Reference 5). The use of inflow control structures in static fan noise tests has reduced the random noise sources that contribute to fan tone noise at the BPF and its harmonics. It also has reduced fluctuations in the fan rotational speed. As a result of these changes (i.e. reduction of random noise sources and stabilization of fan rotational speed) fan tone noise has become dominated by deterministic noise sources and its radiation pattern can be lobular. For these reasons, in tests where detailed directivity information is necessary, a large number of microphones may be required to provide an adequate definition of the tone noise radiation patterns in static tests. The microphone locations used in the static noise tests described in Reference 6 are recommended, and are shown in Figure 3. Pole microphones at 70° and 110° are used for on-line comparison between high frequency segments (f > 5 KHz) of ground and pole microphone data. Noise radiated into angles smaller than 30° and larger than 160° usually contributes very little to aircraft flyover noise.

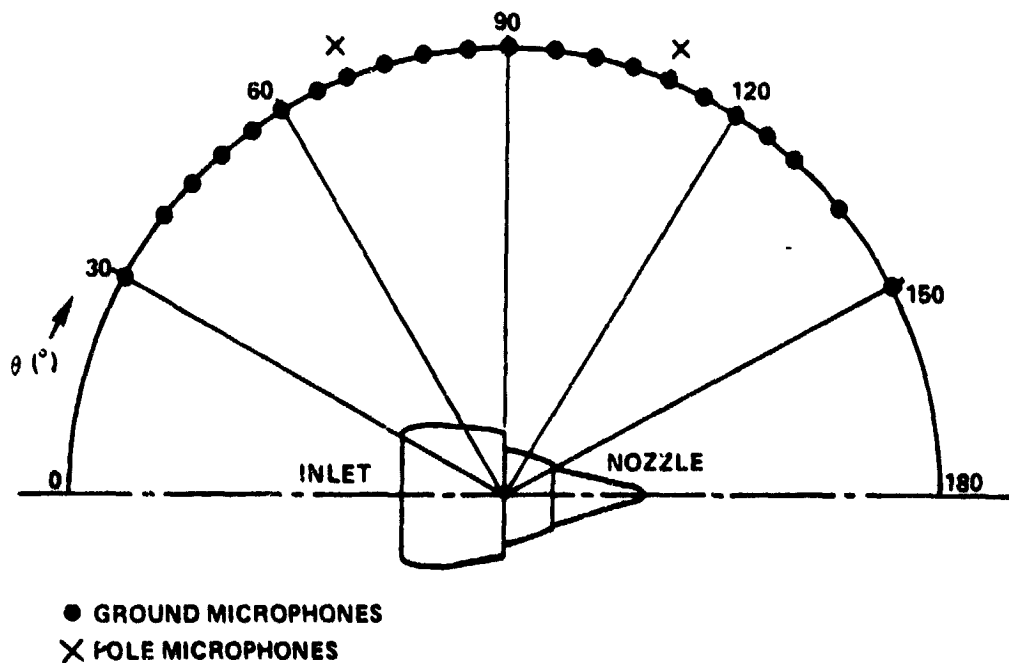
● GROUND MICROPHONES
X POLE MICROPHONES

Figure 3   Microphone Array for Static Fan Noise Tests

One-haif inch condensor microphones are recommended. They should provide essentially flat frequency response from 40 to 10 K Hz at grazing incidence, be relatively insensitive to temperature and humidity variations, and be of such construction that they can be calibrated electrostatically.

The ground microphones are mounted with the diaphragm 1/2 inch above the ground facing downwards over a smooth hard measurement field extending from beneath the engine to about 3 meters beyond the measurement point. The microphone support must be designed to have negligible effects on the sound pressure field. Cables should be routed from the far side of the array to the microphones and should not cross the test arena.

Microphone specifications should be the same as in FAR Part 36 Appendix A.

3.2 Meteorological Instrumentation

Atmospheric conditions within the test arena affect tone noise generation as we l as the sound propagation from the engine to the far-field microphones. The atmospheric conditions are characterized by the following parameters:

p (atm)   static pressure (ambient pressure)

T (^{0}C)   static tempe ature

RH (%)   Relative humidity

V_w (m/s)   Wind velocity

δ (degrees)   Wind direction relative to inlet axis

In a first order approximation the acoustic pressure is proportional to the ambient pressure. For practically all static test conditions correction for static pressure changes are not necessary.

Temperature and humidity affect the atmospheric absorption. Ambient temperature is expected to vary only weakly in a horizontal plane, but it can be a strong function of height above ground. In static tests with ground microphones, it is recommended that the ambient temperature be measrued at several heights between the ground and the engine height. The following temperature measurement locations are suggested: i.e., the microphone heights, at the engine centerline, near the humidity measuring device, and one foot off the measurement surface.

The absolute humidity is not expected to vary significantly within the test arena. The relative humidity will however change with the temperature. Several ambient temperatures(i.e. as specified above), and a single dew point measurement within the test arena are expected to provide sufficient information about the relative humidity distribution. Ambient and dew point temperature measurement accuracy should be $0.3^{\circ}C$. This will provide an acceptable relative humidity accuracy of ± 3 percent.

Wind velocity and direction can affect fan noise sources as well as sound propagation. A low threshold, air bearing cup anemometer provides wind velocity information of sufficient accuracy (± 0.22 m/s between 0.447 and 6.71 m/s). Since wind speed and direction may vary significantly over the duration of a test point, they should be recorded continuously for each test point.

3.3 Engine Performance Instrumentation

Instrumentation for all standard engine performance parameters should be available. Engine performance instrumentation to satisfy general and specific measurement needs are required to ensure stable, repeatable, and comparable engine operating characteristics when conducting noise measurement tests. Noise tests conducted on high bypass ratio fan engines require accurate measurement of several important fan parameters. Among these are fan rpm, fan pressure ratio, fan mass flow rate, fan temperature ratio, engine thrust, and fan exhaust area. Additional engine performance parameters are required when the test is concerned with jet exhaust noise generation. These parameters include nozzle temperatures and pressures, overall pressure ratio, and primary

86

engine exhaust area. A total engine noise test would require at least all of the above mentioned parameters plus any other special flow and aerodynamic parameters that might be required for special noise tests. Care must be taken to ensure that the instrumentation does not affect radiated noise. Ambient conditions of temperature, atmospheric pressure, humidity and wind speed and direction must also be measured as described in Section 3.2, in order that the measured engine performance parameters can be corrected to standard conditions for effective noise measurement comparisons.

4.0 Test Condition Recommendations

In this discussion the term test point is used to describe a time period during which acoustic data are acquired while the engine operates in a stabilized condition.

4.1 Test Point Characteristics

Each test point is characterized by a set of corrected engine parameters (corrected rotational speeds, corrected mass flow rates, component pressure ratios). For typical static test conditions, the relationships between the various corrected engine parameters are unaffected by the ambient atmospheric conditions. A single corrected engine parameter can therefore be selected to characterize the various test points. In static tests concerned with fan noise, it is reasonable to select one of the parameters that describe the thermodynamic cycle of the fan. The corrected fan speed $N1/\sqrt{\Theta}$ which is directly related to the fan tip Mach number is one of the corrected parameters that describes the fan cycle. It is easily measured and provides a reliable signal. It is suggested that $N1/\sqrt{\Theta}$ be used to character.ze the test points in static fan noise tests.

4.2 Engine Operating Point Variability for a Test Point

Engine transients between test points result in very low frequency thermodynamic transients in various engine components. In order to provide stable engine operating conditions at a test point, a stabilization period of at least 2 minutes is recommended before each test point. Unsteady distortions in

87

the inflow field of engines typical for static test conditions cause signifi-
cant fluctuations in the engine operating conditions. These fluctuations are
greatly reduced with an inflow control structure. Without an inflow control
structure corrected speed fluctuations for a test point are typically 1 per-
cent of the corrected fan speed. With an inflow control structure they are
reduced to about 0.3 percent. Corrected fan speed differences between the
various engines on an aircraft in a flyover noise test are typically in the
order of 1 percent of the average corrected fan speed. The reduced corrected
fan speed fluctuations in static tests with inflow control structure will
likely result in lobular directivity patterns at the fan BPF and its harmo-
nics. It is necessary to consider how to use the static data, with its lobular
directivity pattern, to predict flight, which also has lobular directivity
patterns and engine to engine speed variations, which tend to average out the
lobular patterns.

There are two methods to account for this variation. The first method is to
ootain static noise data at many fixed corrected speeds, predict flyover noise
levels at a series of corrected speed values simulating a typical fly- over
speed variation, and average the resulting predictions. The second method is
to simulate the flyover corrected speed variation during the data acquisi-
tion in a static noise test and predict a single flyover noise level from the
static measurement.

The two methods differ fundamentally in the procedure for simulating the cor-
rected speed variation in flyover measurements. In the first method the cor-
rected speed variation is directly simulated by making flight noise predictions
at a series of corrected speeds while in the second method the flyover speed
variation is simulated in the static data acquisition process. The second
method is an approximation to the procedurally correct first method and will
produce the same answer as the first method only if the transformations that
are used to predict flight noise levels from static m. surements are linear.
However, the second method may be more practical to implement.

In addition to being more practical, the second method has two other aovan-
tages. First, analysis of the effect of an inlet control screen on fan noise
directivity has demonstrated that, for a specific source structure, the screen

88

can, if it contains discontinuities, alter the source directivity via diffraction effects. These diffraction effects can be eliminated (i.e., average to zero) if the engine speed is varied slightly to produce a varying source structure. Second, fan noise directivity is very lobular and sensitive to corrected speed, and varying corrected speed slightly during a static test will produce a better estimate of fan noise at a nominal speed than data obtained with corrected speed held strictly constant.

In the past, before the use of an Inflow Control Structure, the fan directivity patterns that were measured were much smoother. Accordingly, problems presented by the lobular directivity patterns were not encountered, and neither of the above methods have been used by Pratt & Whitney Aircraft and Boeing. A variant of the first method has been used where a relatively small number of speed points were used to define the noise versus speed characteristics of the engine, and flight predictions were made for a nominal flight speed. Therefore it is difficult at this time to select one of the methods as being the preferred one. The selection is best made by the user depending on constraints unique to his case, e.g. test time, test costs, available data reduction and processing equipment, etc.

4.3 Temperature and Relative Humidity Restrictions

In flyover testing with its inherently long propagation distances between the source and the microphone, atmospheric absorption has a significant effect on the measured data. In this situation a tight restriction on air temperature and humidity is reqired (FAR Part 36 test window, Figure 4). In static tests the propagation distances are much shorter and a less restrictive test window is acceptable. In the past, static test windows have usually retained the relative humidity limits (20 percent and 95 percent) as well as the no precipitation condition. The lower temperature limit has however frequently been extended to lower temperatures (25 to 30^{0}F), dependent on the expected enviromental conditions. The maximum attenuation limit (12 dB/100 meter at 8 KHz) is frequently waived as well in static tests. A static cest window with relative humidities between 20 and 95 percent, no precipitation and temperature between -5^{0} and 35^{0}C is recommended for static tests, (see Figure 4).
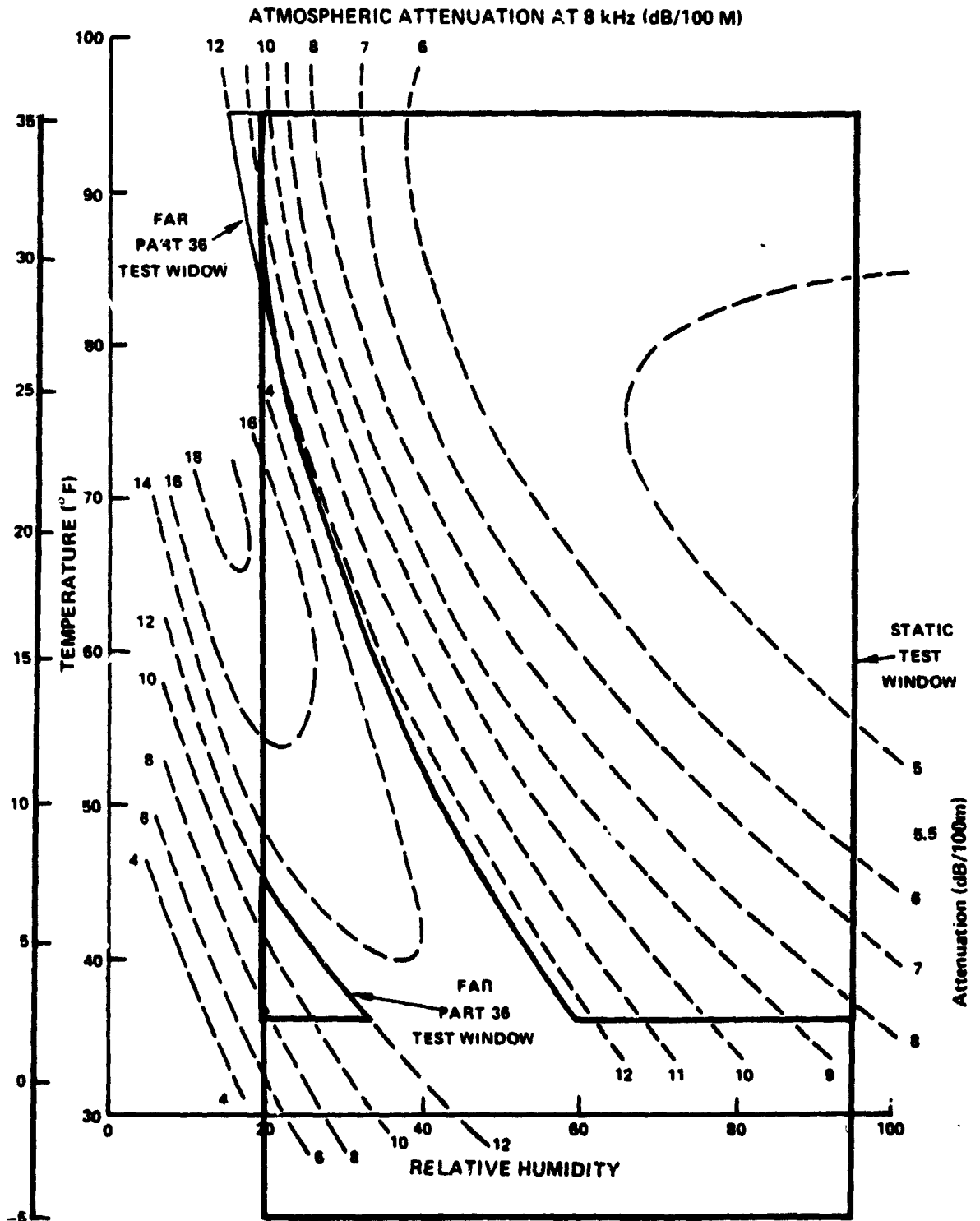
Figure 4   Recommended Test Window

4.4 Wind Velocity and Direction Restrictions

Without an inflow control structure, high wind velocities cause significant
fluctuations in the fan rotor speed. Due to the resulting poor quality of the
engine performance data, the winds from the forward arc have been restricted
by windows like the one shown in Figure 5. Winds from the aft arc result in
increased data scatter, make wind momentum corrections uncertain and may cause
reingestion problems. For these reasons limits on winds from the aft arc are
lower. Temperature distortions in the inflow field persist through an inflow
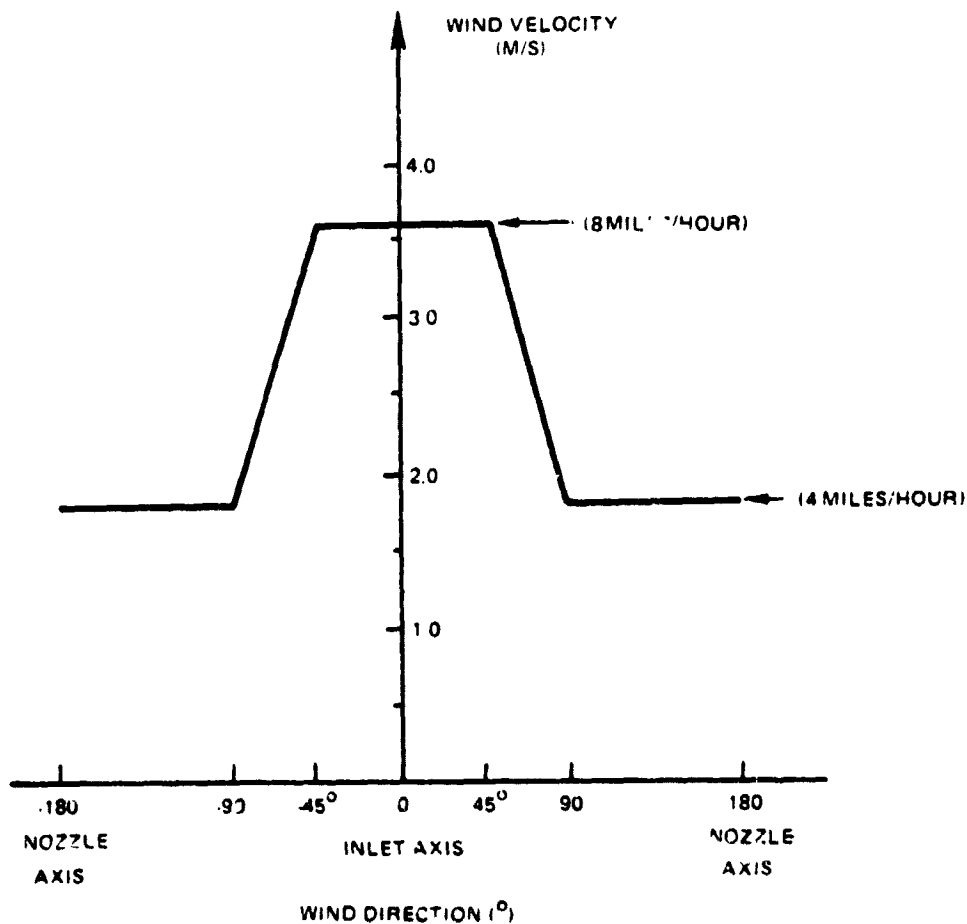control structure and result in velocity distortions at the fan face.

Figure 5   *Typical Wind Limit Used in Static Fan Noise Tests*

In static tests with an inflow control structure the wind limitations should
be based on the following criteria:

- no shadowing of far-field ground microphones

- no reingestion

Observation of the on-line 1/3 OB spectra from the pole and ground microphones
at the same angular location provides information about the first limit. If
the difference of the spectrum levels in the high frequency range ($f > 5$ kHz)
between the ground microphone and the pole microphone fluctuate or become
significantly less than 3 dB, then ground microphone shadowing has occurred
and the acoustic data is not acceptable. Extensive testing within the wind
envelope shown in Figure 5 has prevented the occurrence of ground microphone
shadowing in all tests.

The reingestion problem has not been studied in detail. The nozzle flows act
as ejectors and induce ambient air into the jet flows. This might result in
higher acceptable wind limits for the aft arc without excessive temperature
distortions. In a first order approximation the velocity distortion at the fan
face resulting from an ambient temperature distortion can be estimated based
on the isentropic flow equations. The acceptable temperature distortion based
on the above equation and a velocity distortion limit of 0.2 percent is in the
order of $1^{\circ}C$.

It is recommended that the wind limits presented in Figure 5 be used in static
tests.

92

List of Symbols - Appendix II

Symbol	Units	Description
A	M^2	effective fan nozzle area
a	M	large half diameter of ellipse
b	M	small half diameter of ellipse
f	S^{-1}	frequency
M_∞	--	aircraft Mach number
m	--	spinning order of duct mode
$\dot{m}$	kg/S	nozzle mass flow rate
$N1$	rpm	fan rotational speed
OB	--	octave band
p	kg/MS^2	static pressure
p_t	kg/MS^2	total pressure
RH	$\%$	relative humidity
R	$M^2/S^2\ ^oK$	gas constant
R_o	M	inlet throat radius
T	^oK	static temperature
T_t	^oK	total temperature
V_w	M/s	wind velocity
δ	degrees	wind direction
γ	--	specific heat ratio of air
θ	--	ambient static temperature $(^oK)/288^oK$
φ	degrees	polar angle

References

Appendix II

1. Ganz, U. W., "Parametric Study of the Fan Inflow Field in Static and Flight Tests", Boeing document D5-49669, May 1980.

2. Mathews, D. C. and Nagel, R. T., "Inlet Geometry and Axial Mach Number Effects on Fan Noise Propagation", AIAA Paper 73-1022, October 1973.

3. Clark, T. L., "Investigation of the Effects of Inlet Shape on Fan Noise Radiation", Final Report, NASA Contract NAS1-15394, January 1981.

4. Walker, D. Q., "Some Effects of the Local Atmosphere Upon Acoustic Data from Full Scale Static Engine Tests", Boeing document D6-4060 TTN, Sept 1972.

5. Lanter, S. K., etal, "Flyover Noise of a Widebody Aircraft", Presented at the ASA Conference in Salt Lake City, November, 1979.

6. Atvars, Y. and Rogers, D. F, "The Development of Inflow Control Devices for Improved Simulation of Flight Noise Levels During Static Testing of a HBPR Turbofan Engine", AIAA paper 80-1024, June, 1980.

APPENDIX III
TEST CONFIGURATIONS

The following test configurations were used in assessing the procedures manual by comparing measured static data projected to flight with measured flight data. The engine used in the static and flight tests was a JT9D-7 engine, equipped with a Boeing -200 nacelle. The nacelle was hardwalled for both the static and flight cases. The flight data was obtained from JT9D's on a Boeing 747 airplane with all engines hardwalled.

Four speeds were analyzed, and data were selected for the fan speeds used during the flight test program. Static data for these speeds was obtained by interpolation, as a function of speed. The flight test conditions used for the assessment are defined in the following:

Flight Condition	Nominal Corrected N1 (RPM)	Altitude at Overhead (M)	Flight Velocity (M/S)	Climb Angle	Pitch of Aircraft	Nacelle Angle Relative To Aircraft
Approach 30° Flap	2296	113	80	-3^{0}	$.8^{0}$	2.3^{0}
Approach 25° Flap	2327	113	80	-3^{0}	$.8^{0}$	2.3^{0}
Takeoff	3270	244	100	4.97^{0}	14.2^{0}	2.3^{0}
Cutback	3008	244	100	2.29^{0}	11.0^{0}	2.3^{0}

C-2

The flight data was corrected as follows.

1. Raw data corrected to 77°, 70% relative humidity FAA day.
2. Data is corrected to the flight path cited above.
3. Microphone incidence angle correction was applied to the data.
4. The data was time averaged over .5 second intervals. Values of the time averaged data for the static measurement angles used in the assessment of section 4.4 were obtained by interpolation knowing the relationship between angle and flyover time.

96

APPENDIX IV
PLANS FOR EVALUATION OF INTERIM PROCEDURES REPORT USING JT15D DATA

BACKGROUND:

The lack of agreement between measured inflight fan noise characteristics and predictions based on ground static data is a problem that has hindered the development of lower noise fans. Investigations by NASA, P&WA, Boeing and others have shown that spurious fan tones are generated in static tests from interactions of the fan with inflow distortions caused by wakes from test stand structure, vortices from the ground and other surfaces, and greatly distorted atmospheric turbulence. In October 1977 Pratt and Whitney Aircraft with Boeing as a subcontractor initiated work in the Forward Speed Effects on Fan Noise Contract (NAS1-15085) from NASA Langley. The major effort in this contract, which is discussed in this report, was the development of an Interim Procedures Report that includes a design system for Inflow Control Structures that would be used during static tests to remove inflow distortions unique to the static test environment. An assessment of the Inflow Control Structure design and corrections defined to extrapolate the static data to flight was included as a contract task. This assessment was based on 747/JT9D static and flyover data and is discussed in section 4.4. To validate the general applicability of the procedures developed in this contract it would be useful to assess these procedures using data from a different size engine and installation. This can be accomplished using NASA JT15D test program data, including data from completed static and wind tunnel tests and planned flight and fan rig tests.

Included as part of the Contract Program Coordination task is a requirement to propose JT15D program plans for further evaluation and improvement of the static test procedures developed. These plans are to include flight and fan rig test requirements. The technology base developed in the current contract together with the efforts outlined below involving use of NASA JT15D data will provide a final procedures report for static, wind tunnel, and rig testing verified for both large and small scale engines.

APPROACH:

A combined analytical and experimental program is suggested for the further evaluation and improvement of static test procedures developed in the current contract. Program elements are outlined below:

1. Inflow control structure design procedures developed in the current con-
   tract will be used to define pertinent characteristics of an Inflow
   Control Structure design for the JT15D engine. Inflow control structure
   designs tested by NASA Lewis will be assessed by comparing their charac-
   teristics with the recommended characteristics.

2. Static test procedures defined in the interim report will be assessed
   using JT15D acoustic and blade mounted transducer (BMT) data.

   o   Inflow control structure design procedures will be assessed by com-
       paring static and flight blade mounted transducer data and consider-
       ing the results of the Task 1 comparisons.

   o   An overall assessment of the procedures will be performed by compar-
       ing measured JT15D flight acoustic data with flight noise levels
       predicted from static data using the procedures developed in this
       contract to project static data to flight. This assessment will be
       performed to the level of detail possible based on data availability.

   o   The procedures, including Inflow Control Structure design and static-
       to-flight correction factors will be updated as appropriate, based on
       results of the above assessment.

3. If it is concluded that relevant design characteristics are not satisfied
   by an existing Inflow Control Structure and/or additional testing is
   necessary to assess further the procedures report, a static test program
   will be defined and the evaluations described in Task 2 will be repeated
   using the newly acquired data and the procedures will be updated further.

4. Corrections will be defined that should be applied to engine data obtained in the NASA Ames wind tunnel to allow comparison with flight data.

5. An assessment will be made of the effectiveness of Ames wind tunnel testing as a means of simulating inflight fan noise by comparing predicted flight levels, based on Ames JT15D data corrected by the factors defined in item 4 above, with measured JT15D flight data. Correction factors will be updated if appropriate.

6. An assessment will be made of the applicability of the static test procedures to fan rig testing by comparing data from NASA JT15D rig tests, obtained and corrected in accordance with the proposed procedures, with NASA flight test data. Appropriate additional corrections and requirements will be defined.

7. A factor not considered by the current contract is the static simulation of in-flight mean flow velocity throughout the inlet and at the fan face, boundary layer conditions at the fan face, and the effect on fan noise generation and propagation of inlet droop. The importance of accounting for these factors in static testing should be assessed.

8. If the item 7 assessment indicates that those effects are important in static testing, inlet design and boundary layer control methods will be developed to provide the proper simulation.